Molecular Plant • Volume 7 • Number 5 • Pages 792–813 • May 2014 RESEARCH ARTICLE

iNID: An Analytical Framework for *I*dentifying *N*etwork Models for *I*nterplays among *D*evelopmental Signaling in *Arabidopsis*

Daeseok Choi[a], **Jaemyung Choi**[b], **Byeongsoo Kang**[c], **Seungchul Lee**[a], **Young-hyun Cho**[b], **Ildoo Hwang**[b,d,1], and **Daehee Hwang**[a,c,e,1]

a School of Interdisciplinary Bioscience and Bioengineering, POSTECH, 790-784, Pohang, Republic of Korea
b Department of Life Sciences, POSTECH, 790-784, Pohang, Republic of Korea
c Department of New Biology, DGIST, Daegu, 711-873, Republic of Korea
d Division of Integrative Biosciences and Biotechnologies, POSTECH, 790-784, Pohang, Republic of Korea
e Center for Systems Biology of Plant Senescence and Life History, Institute for Basic Science, DGIST, Daegu, 711-873, Republic of Korea

ABSTRACT Integration of internal and external cues into developmental programs is indispensable for growth and development of plants, which involve complex interplays among signaling pathways activated by the internal and external factors (IEFs). However, decoding these complex interplays is still challenging. Here, we present a web-based platform that *i*dentifies key regulators and *N*etwork models delineating *I*nterplays among *D*evelopmental signaling (iNID) in *Arabidopsis*. iNID provides a comprehensive resource of (1) transcriptomes previously collected under the conditions treated with a broad spectrum of IEFs and (2) protein and genetic interactome data in *Arabidopsis*. In addition, iNID provides an array of tools for identifying key regulators and network models related to interplays among IEFs using transcriptome and interactome data. To demonstrate the utility of iNID, we investigated the interplays of (1) phytohormones and light and (2) phytohormones and biotic stresses. The results revealed 34 potential regulators of the interplays, some of which have not been reported in association with the interplays, and also network models that delineate the involvement of the 34 regulators in the interplays, providing novel insights into the interplays collectively defined by phytohormones, light, and biotic stresses. We then experimentally verified that BME3 and TEM1, among the selected regulators, are involved in the auxin–brassinosteroid (BR)–blue light interplay. Therefore, iNID serves as a useful tool to provide a basis for understanding interplays among IEFs.

Key words: transcriptome analysis; network analysis; signal interplays; development; *Arabidopsis*.

INTRODUCTION

Plants, which are sessile, constantly revise their developmental programs to cope with changing environments during growth and development. Integration of internal and external cues into the developmental programs is thus essential. This integration involves complex interplays among signaling pathways activated by both internal and external factors (IEFs), leading to coordination in developmental outputs, such as germination, elongation, and maturation, over the developmental stages. For example, plants perceive season, temperature, and their developmental status to determine a precise timing of flowering for successful reproduction. Regulation of the timing of flowering involves complex interplays among external (e.g. photoperiod, vernalization, and temperature) and internal factors (e.g. gibberellins (GA)) (Srikanth and Schmid, 2011).

Identification of key regulators for the interplays and biological networks delineating the interplays mediated by these regulators is critical to understand coordinated controls by IEFs during plant development. Genetics approaches have been used to investigate the interplays between IEFs. For example, Xi et al. (2010) identified a key regulator for

[1] To whom correspondence should be addressed. D.H. Department of New Biology, DGIST, 50-1, Sang-Ri, Hyeonpung-Myeon, Dalseong-Gun, Daegu 711-873, Republic of Korea. E-mail dhwang@dgist.ac.kr, tel. 82-53-785-1840, fax 82-53-785-1819. I.H. Department of Life Sciences, POSTECH, San 31, Hyoja-dong, Nam-gu, Pohang, Kyungbuk, 790-780, Republic of Korea. E-mail ihwang@postech.ac.kr, tel. 82-54-279-2291, fax 82-54-279-8409.

doi:10.1093/mp/sst173, Advance Access publication 31 December 2013
Received 25 June 2013; accepted 16 December 2013

seed germination, *mother of FT AND TFL1* (*MFT*), which integrates the signals from abscisic acid (ABA) and GA (Xi et al., 2010). Also, several studies (Moon et al., 2003; Hisamatsu and King, 2008) used genetics approaches to identify flowering time regulators, such as *FT* and *SOC1*, as the integrators of the signals from photoperiod, vernalization, and GA. However, these approaches require huge amounts of labor and time, and also commonly provide relationships among a limited number of molecules. Thus, it is often challenging to search for key regulators involved in the interplays among multiple IEFs, leading to the limited capability of decoding biological networks for the interplays among a large number of IEFs. Therefore, there has been a need for an alternative approach that can effectively identify both key regulators and biological networks for the interplays.

Gene expression analysis has been offering new opportunities for identifying key regulators and networks associated with the interplays. Several tools for analysis of transcriptome data and/or network analysis have been developed (Supplemental Table 1). First, BAR Expression angler (Toufighi et al., 2005) and Genevestigator (Hruz et al., 2008) provide tools to explore gene expression profiles and identify co-expressed genes. However, they provide no tools to generate biological networks and identify key regulators. Second, CSB.DB (Steinhauser et al., 2004), ATTED-II (Obayashi et al., 2007), CORNET (De Bodt et al., 2010), and CorTo (Giorgi et al., 2013) provide tools to identify co-expressed genes and generate biological networks. Also, the interactome databases, AtPID (Cui et al., 2008), AtPIN (Brandao et al., 2009), AtPAN (Chen et al., 2012), or GeneMANIA (Mostafavi et al., 2008), can be used to generate biological networks. However, they provide no tools to identify key regulators based on the networks. Third, VirtualPlant (Katari et al., 2010) provides tools to identify differentially expressed genes (DEGs), generate networks, and identify network statistics scores for the nodes in the networks. However, these scores provide no statistical framework to select key regulators in the networks. Thus, all these tools, which are not specifically designed to analyze the interplays among multiple IEFs, are still lack of statistical tools to identify key regulators and network models associated with the interplays among IEFs.

Here, we present a web-based analytical framework that identifies key regulators and Network models delineating Interplays among Developmental signaling (iNID). iNID provides (1) a comprehensive database of gene expression profiles and interactomes in *Arabidopsis* and (2) three analytical tools for a series of analyses to identify key regulators and network models for interplays among multiple IEFs (Figure 1). The database contains 488 gene expression profiles collected after treatments with 41 IEFs and 1 171 417 interactions including protein–protein interactions (PPIs), protein–DNA interactions (TF–target; PDIs), protein–metabolite interactions (PMIs), genetic interactions (GIs), etc. The three analytical tools were developed for (1) identification of the genes related to the interplay among a selected set of IEFs; (2) selection of key regulators mediating the interplay from the interplay-related genes; and (3) development of network models for the interplay using the key regulators and their associated pathways. iNID is available at http://sbm.postech.ac.kr/inid (accessed 24 January 2014).

RESULTS

Transcriptomic Data in iNID

For investigation of interplays among various IEFs, iNID provides 41 time-course gene expression data sets (536 arrays) that were generated after treatments of the following four groups of IEFs (Table 1): (1) eight phytohormones: ABA, auxin, brassinosteroid (BR), cytokinin (CK), ethylene (ET), GA, jasmonic acid (JA), and salicylic acid (SA) (van Leeuwen et al., 2007; Goda et al., 2008) (GSE39384, E-TABM-51); (2) four different wavelengths of light (red, far-red, blue, and white lights; GSE5617); (3) abiotic stresses, including cold (GSE5621), drought (GSE5624), genotoxic (GSE5625), heat (GSE5628), osmotic (GSE5622), salt (GSE5623), UV-B (GSE5626), and wounding (GSE5627) (Kilian et al., 2007); and (4) biotic stresses, including *Botrytis cinerea* (GSE5684), *Phytophthora infestans* (GSE5616), *Erysiphe orontii* (GSE5686), pathogen-derived elicitors (hairpin Z, GST-NPP1, Flg22, and LPS; GSE5615), and six different *Pseudomonas syringae* strains (pv. maculicola strain ES4326, pv. maculicola strain ES4326 avrRpt2 (GSE5685), pv. tomato DC3000, pv. tomato avrRpm1, pv. tomato DC3000 hrcC$^-$, and pv. phaseolicola (ME00331)).

After treatments of these four groups of IEFs, gene expression profiles were measured at various developmental stages and tissues over time (Table 1). Gene expression profiles under conditions treated with seven of the eight phytohormones (ABA, auxin, BR, CK, ET, GA, and JA) and light were generated from seedlings in early stages (i.e. 7- and 4-day-old seedlings, respectively). After SA treatments, gene expression profiles were obtained from 5- or 6-week-old vegetative leaves. Gene expression profiles under abiotic stress conditions were measured from 18-day-old shoot and root tissues. Using the data from these two different tissues, we can examine tissue-specific responses to the abiotic stresses. On the other hand, gene expression profiles under biotic stress conditions were generated from 4–5-week-old leaves (GSE5684, ME00331, GSE5616, and GSE5686) and distal leaf tissues inoculated with the above pathogens (GSE5685). Using these data, molecular signatures associated with systemic acquired resistance in the leaves can be investigated. However, the analysis of the data sets generated from different developmental stages, different tissues, and under different experimental conditions may lead to misinterpretation of the data due to the variations from different stages and tissues (see the 'Discussion' section for details).

For each data set, iNID provides the significance (adjusted *P*-values and false discovery rates; FDR) that each gene is differentially expressed over time by the corresponding IEF.

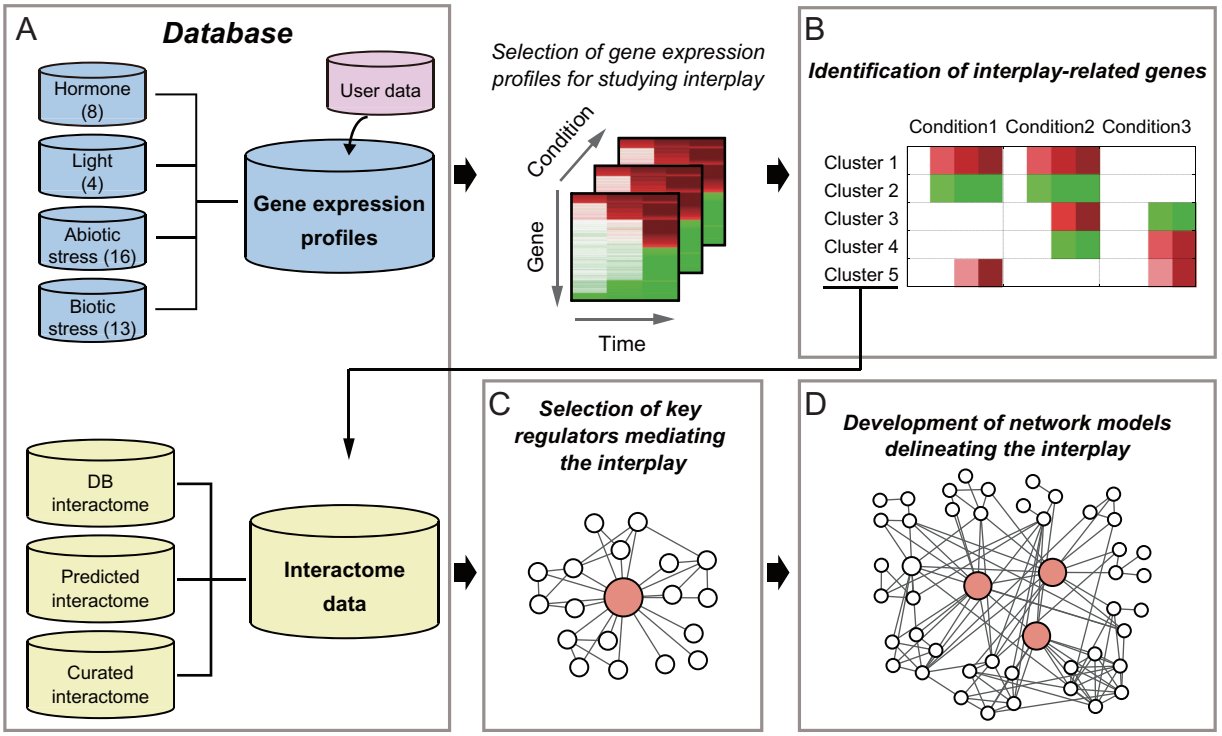

Figure 1. Database and Analytical Tools in iNID for Investigating Interplays among IEFs.

(A) Database including (1) 41 time-course data sets collected after treatments of phytohormones, light, and abiotic and biotic stress; and (2) interactomes obtained from public databases and interaction data curated from previous literatures and gene expression data of mutants. The numbers of data sets in each category of IEFs are denoted in parentheses. From this database, gene expression profiles related to the interplay being investigated are selected. A three-dimensional (time, gene, and condition) heat map shows example up- (red) and down-regulated (green) genes.
(B) Identification of interplay-related genes showing differential expression patterns in the selected data sets (Conditions). Example interplay-related clusters and their expression patterns are shown.
(C) Selection of key regulators mediating the interplay. An example key regulator (a large node in the center) with a large number of interactors is shown.
(D) Development of network models for the interplay using the key regulators and their associated pathways. An example network model for the interplay is shown. The network model includes the three key regulators (large nodes in the center).

To identify DEGs from individual data sets on the common statistical basis, we re-analyzed all data sets and selected DEGs with $P <$ a cut-off (e.g. P or FDR < 0.05) using the method we previously reported (Storey and Tibshirani, 2003; Hwang et al., 2009). For a list of genes, the changes in their expression under the IEF-treated conditions can be explored using 'Quick search' in iNID (Supplemental Figure 1A). In addition, for analysis of a new gene expression data set not included in iNID, iNID provides an interface that imports P-values and fold-changes pre-computed using the above method (available in the iNID website) or users' own statistical methods (Supplemental Figure 1B). Using this interface, users can investigate the interplays between their own data sets and the ones in iNID.

Interactome Data in iNID

iNID provides interactomes (Figure 2A and Supplemental Figure 2) that comprise (1) interactomes collected from 10 databases or resources (DB interactome in Figure 2A), TAIR (Lamesch et al., 2012), BIOGRID (Stark et al., 2011), BIND (Bader et al., 2003), Intact (Kerrien et al., 2007), AGRIS (Yilmaz et al., 2011), TRANSFAC (Matys et al., 2003), KEGG (Kanehisa et al., 2006), multi-network (Gutierrez et al., 2007), AtORFeome2.0 (Braun et al., 2011), AtPIN (Brandao et al., 2009), and PPIN-1 (Mukhtar et al., 2011); (2) interactomes predicted by various methods (Predicted interactome in Figure 2A; e.g. PPIs predicted from homologous interactions in other species) in Aranet (Lee et al., 2010b), Interactome2.0 (Geisler-Lee et al., 2007), and multi-network (Gutierrez et al., 2007); and (3) interactomes manually curated from previous literatures (Curated interactome in Figure 2A). iNID contains in a total of 1 171 417 interactions for 27 103 molecules. The 'DB interactome' includes a total of 50 293 interactions: (1) 21 556 PPIs, (2) 80 GIs, (3) 11 548 PDIs, (4) 16 990 PMIs, and (5) 119 microRNA–target interactions. The 'Predicted interactome' includes a total of 1 119 519 interactions: (1) 253 520 PPIs, (2) 22 590 GIs, (3) 1625 PDIs, (4) 56 protein–RNA interactions (PRIs), and (5) 371 781 functional interactions. Finally, the 'Curated interactome' (Supplemental Data 1) include a total of 27 112 interactions: (1) 14 086 PPIs, (2) 1407 GIs, (3) 11 559

Table 1. Transcriptomes Collected after Treatments of IEFs in iNID.

Category	Array ID	Condition	# DEGs[a]	Sample	Time point	Reference/ database
Hormone	GSE39384[b]	Abscisic acid	1096	7-day-old seedlings	30 min, 1 h, 3 h	Goda et al., Plant J. (2008)
		Auxin	1049			
		Brassinosteroid	754			
		Cytokinin	924			
		Ethylene	752			
		Gibberellin	459			
		Jasmonic acid	1132			
	E-TABM-51[c]	Salicylic acid	901	5–6-week-old leaves	4 h, 28 h, 52 h	van Leeuwen et al., Plant Cell (2007)
Light	GSE5617[b]	Red	1143	4-day-old seedlings	45 min, 4 h	At GenExpress
		Far-red	1473			
		Blue	1429			
		White	1527			
Abiotic stress (shoot)	GSE5621[b]	Cold	1272	Shoot of 18-day-old plants	30 min, 1 h, 3 h, 6 h,12 h, 24 h	Kilian et al., Plant J. (2007)
	GSE5624[b]	Drought	1028			
	GSE5622[b]	Osmotic	1087			
	GSE5623[b]	Salt	1162		15 min, 30 min, 1 h,3 h, 6 h, 12 h, 24 h	
	GSE5625[b]	Heat	1370			
	GSE5626[b]	UV-B	1216			
	GSE5627[b]	Wounding	1053			
	GSE5628[b]	Genotoxic	881			
Abiotic stress (root)	GSE5621[b]	Cold	1155	Root of 18-day-old plants	30 min, 1 h, 3 h, 6 h,12 h, 24 h	Kilian et al., Plant J. (2007)
	GSE5624[b]	Drought	970			
	GSE5622[b]	Osmotic	1075			
	GSE5623[b]	Salt	1150		15 min, 30 min, 1 h, 3 h, 6 h, 12 h, 24 h	
	GSE5625[b]	Heat	1339			
	GSE5626[b]	UV-B	1052			
	GSE5627[b]	Wounding	874			
	GSE5628[b]	Genotoxic	936			
Biotic stress	GSE5685[b]	*P. syringae* pv. maculicola ES4326	1064	4-week-old plants	4 h, 8 h, 16 h, 24 h, 48 h	AtGenExpress
		P. syringae pv. maculicola ES4326 avrRpt2	1010			
	ME00331[d]	*P. syringae* pv. tomato DC3000	1378	5-week-old plants	2 h, 6 h, 24 h	
		P. syringae pv. tomato avrRpm1	1278			
		P. syringae pv. tomato DC3000 hrcC$^-$	1249			
		P. syringae pv. phaseolicola	1188			

Table 1. Continued

Category	Array ID	Condition	# DEGs[a]	Sample	Time point	Reference/ database
	GSE5615[b]	Pathogen-derived elicitors: hairpin Z	1493	5-week-old plants	1 h, 4 h	
		Pathogen-derived elicitors: GST-NPP1	1475			
		Pathogen-derived elicitors: Flg22	1523			
		pathogen-derived elicitors: LPS	790			
	GSE5684[b]	*Botrytis cinerea*	849	4-week-old plants	18 h, 48 h	
	GSE5616[b]	*Phytophthora infestans*	1588	5-week-old plants	6 h, 12 h, 24 h	
	GSE5686[b]	*Erysiphe orontii*	1361	31-day-old plants	6 h, 12 h, 18 h, 24 h, 2 d, 3 d, 4 d, 5 d	

[a] Differentially expressed genes (DEGs) with $P < 0.01$ and absolute $\log_2$fold-change > 0.58. The data sets are available from [b]NCBI GEO database, [c]EBI Arrayexpress, and [d]TAIR.

PDIs, (4) 45 PMIs, (5) 10 microRNA–target interactions, and (6) five PRIs. In addition, by analyzing 389 gene expression data sets obtained from 263 transgenic plants (Supplemental Data 2), we also identified 469 947 genetic associations between mutated genes and DEGs in the mutants, compared to wild-types (Supplemental Data 3).

To facilitate interpretation of network models for the interplays, iNID provides a pathway model generated using the curated interactions for each of which experimental evidence was previously reported and that are thus relatively reliable to the DB and Predicted interactomes (Figure 2A). Among 12 137 molecules with the curated interactions, 1887 molecules are mapped into 22 known pathways (Figure 2B) based on the molecule–pathway association reported in the literatures and AHD2.0 database (Jiang et al., 2011). The 22 pathways comprise (1–9) phytohormones pathways (ABA, auxin, BR, CK, ET, GA, JA, SA, and strigolactone), (10) light signaling pathways, (11) defense-related pathways, (12) flowering, (13) 26S proteasome, (14) cell division, (15) cell death, (16) chromatin remodeling, (17) embryo development, (18) mitogen-activated protein kinase (MAPK) signaling, (19) senescence, (20) shoot apical meristem development, (21) stress, and (22) trichome development pathways. Each pathway model is then defined by the molecules mapped to the pathway and the curated interactions among them. For example, the defense-related pathway model (Figure 2C) includes the molecules involved in pathogen effectors, receptors, resistance (R)-genes, R-gene-interacting genes, MAPK signaling components, and defense regulators, and the interactions among these molecules. Based on this pathway model, among the 22 pathways, iNID provides pathways represented by the genes in network models delineating the interplays among IEFs (see case studies below).

Identification of Key Regulators and Network Models for Interplays Using iNID

In addition to the above resources, iNID provides an array of analytical tools for identifying interplay-related genes, selecting key regulators for the interplays, and reconstructing network models for the interplays (Figure 1). To demonstrate the utility of the data resources and the analytical tools, we applied iNID to the two case studies to understand interplays among (1) two phytohormones, auxin and BR, and blue light and (2) eight phytohormones and defense responses to nine pathogens.

Case Study 1: Interplays among Auxin, BR, and Blue Light

Light and phytohormones are indispensable in growth and development of plants (Alabadi and Blazquez, 2009; Lau and Deng, 2010). Various developmental processes, such as phototropism and hypocotyl growth, involve the action of blue light, auxin, and BR (Hardtke et al., 2007; Jiao et al., 2007). Several studies identified the genes involved in the interplays among these three factors: (1) NPH3 (Wan et al., 2012) between blue light and auxin, (2) GATA2 (Luo et al., 2010) between blue light and BR, and (3) BIN2 and ARF2 (Vert et al., 2008) between auxin and BR. However, there has been no systematic approach for identifying the components mediating the interplays among auxin, BR, and blue light. Moreover, biological networks describing the interplays among these IEFs have been rarely explored. Thus, we applied iNID to

A

Category	Interaction type	# Interactions	Reference
DB interactome	protein-protein interaction	21,556	TAIR, BIOGRID, BIND, Intact, TRANSFAC, multinetwork, AtPIN, AtORFeome2.0*, PPIN-1*
	genetic interaction	80	BIOGRID
	protein-DNA interaction	11,548	AGRIS, TRANSFAC
	protein-metabolite interaction	16,990	KEGG, multinetwork
	microRNA-target interaction	119	multinetwork
	total	50,293	
Predicted interactome	protein-protein interaction	253,520	Interactome2.0, multinetwork
	genetic interaction	22,590	Interactome2.0
	protein-DNA interaction	1,625	multinetwork
	protein-RNA interaction	56	Interactome2.0
	functional interaction	371,781	Aranet
	microarray genetic interaction	469,947	
	total	1,119,519	
Curated interactome	protein-protein interaction	14,086	
	genetic interaction	1,407	
	protein-DNA interaction	11,559	
	protein-metabolite interaction	45	
	microRNA-target interaction	10	
	protein-RNA interaction	5	
	total	27,112	
	Total	1,171,417	

Molecule type	# Molecules
Gene	13,622
Metabolite	1,147
Effector	83
MicroRNA and siRNA	27
Locus	19
total	14,898
Gene	16,832
Locus	4
total	16,836
Gene	12,068
Metabolite	24
Effector	18
MicroRNA and siRNA	10
Locus	17
total	12,137
Total	27,103

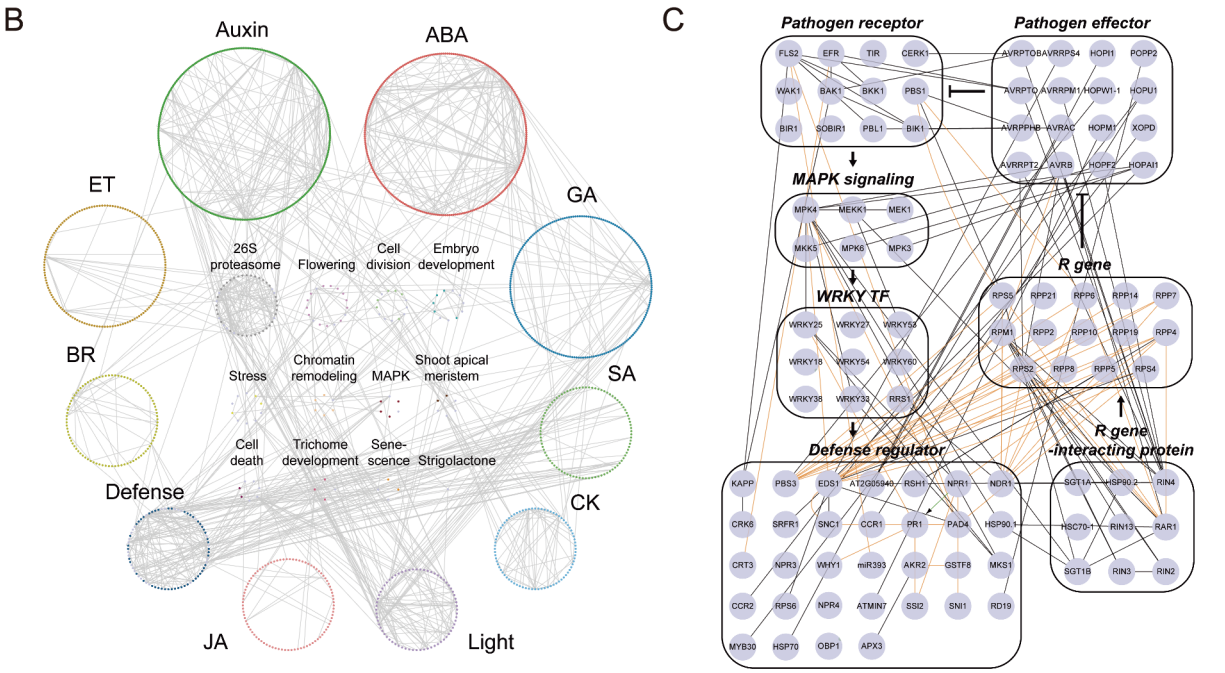

Figure 2. *Arabidopsis* Interactomes in iNID.

(A) The statistics of three groups of interactomes, each of which was further categorized into subgroups of interactions. For example, the total 50 293 interactions collected from public DBs (DB interactome) can be further divided into five types of interactions.

(B) The pathway model constructed from the curated interactome, including eight phytohormones pathways (ABA, auxin, BR, CK, ET, GA, JA, and SA), light signaling pathways, flowering, 26S proteasome, and defense-related pathways. Colors indicate different pathways.

(C) A network model showing defense-related pathways. Black line, PPI; green line, PDI; orange line, GI.

systematically identify key regulators and network models for the interplays among these IEFs.

Identification of the Genes Related to Interplays among Auxin, BR, and Light

We first selected gene expression profiles generated after treatments of auxin, BR, and blue light using the 'Selection of datasets' tool in the 'Start analysis' page of iNID (red arrow in Figure 3A). DEGs in these conditions were identified as the genes with $P < 0.05$ and absolute $\log_2$-fold-change > 0.58 (1.5-fold) using the 'Options' in the 'Identification of interplay-related genes' tool (blue arrow in Figure 3A). The Venn diagram (Figure 3B) shows 2203, 2158, and 2728 DEGs identified from auxin, BR, and blue light data sets, respectively. Among the DEGs, 281 genes are shared in all three conditions, and 1174 genes (443 + 432 + 299 genes in Figure 3B) are

Figure 3. Identification of the Genes Related to Interplays between Phytohormones, Auxin and BR, and Blue Light.

(A) The interface for selecting data sets related to auxin, BR, and blue light (left panel). DEGs were identified as the genes with $P \leq 0.05$ and absolute $\log_2$-fold-change ≥ 0.58 (1.5-fold) at least one condition (right panel). The selected data sets are shown (middle panel).

(B) The Venn diagram showing the relationship between DEGs in auxin, BR (brassinosteroid), and blue light-treated (blue) conditions (left panel). The input gene lists are shown (middle panel). Each set of the DEGs in the Venn diagram can be selected for further analyses (right panel): in case study 1, 281 genes (Set G) were selected (underlined) and used for 'Pattern analysis' (orange arrow).

(C) The expression patterns related to interplays among auxin, BR, and blue light, and the numbers of genes and regulators (TF- transcription factors, SIG- signaling molecules, and REG- other regulators) included in each cluster. Red and green, up- and down-regulation, respectively, in individual selected data sets. The GO biological processes represented by the genes in the clusters can be performed using 'Related biological processes'. See text for the arrows, boxes, or links.

shared in two of the three conditions. In contrast, 1047, 1135, and 1716 genes showed auxin-, BR-, and blue-light-specific expression changes, respectively. A fundamental assumption in iNID is that the genes showing shared differential expression under multiple conditions are likely to be associated with the interplays among the corresponding IEFs (Nemhauser et al., 2006; Chan, 2012). Thus, the significant numbers of the four sets of the shared DEGs (e.g. $P < 10^{-5}$ for 281 genes in Figure 3B) indicate potential interplays among auxin, BR, and blue light.

Among the shared DEGs, we focused on the 281 DEGs shared in all three conditions. Different increased or decreased expression patterns of the 281 DEGs under the three conditions reflect diverse modes of interplays among these three IEFs. For investigation of the modes of the interplays, iNID provides two clustering methods—pattern analysis and the non-negative matrix factorization (NMF) method (Kim et al., 2011) (see 'Clustering' box in Figure 3A)—due to their complementary nature (see the 'Methods' section for further detail) (Devarajan, 2008). In this case study, among the two methods, we used 'Pattern analysis' (orange arrow in Figure 3B). This analysis grouped the 281 shared DEGs into eight clusters (C1 to C8 in Figure 3C), reflecting eight different modes of the interplays. The largest C1 with 96 genes (34% of the 281 DEGs) showed up-regulation by auxin and BR, but down-regulation by blue light, whereas C3 showed the opposite expression pattern. Thus, C1 and C3 reflect an antagonistic interplay between light and the two hormones. Pairs of the other clusters reflect different relationships among the three IEFs: (1) C2 and C6 showed another antagonistic interplay between auxin and the other IEFs (BR and blue light); (2) C4 and C8 showed the other antagonistic interaction between BR and the other IEFs (auxin and blue light); and (3) C5 and C7 showed the synergistic interplays among the three IEFs. With the cluster navigator (green arrow in Figure 3C), iNID provides information of the genes in the cluster (i.e. names, descriptions, and interactors of the genes, and previous publications associated with the genes), as well as time-course $\log_2$-fold-changes, significances (adjusted *P*-values and FDRs), and a heat map showing differential expression of the genes under the three conditions (Supplemental Figure 3). Also, with the tool of 'Related biological processes' (magenta arrow in Figure 3C), iNID provides cellular processes represented by the genes in each cluster (Supplemental Figure 4).

Selection of Key Regulators Mediating Auxin–BR–Light Interplays

It has been demonstrated that a hub-like regulator with a large number of interactors can serve as a key regulator (Barabasi and Oltvai, 2004; Barabasi et al., 2011). Based on this concept, for every gene in each cluster, iNID computes the numbers of first and second interacting neighbors among the 281 DEGs. iNID provides two methods—the non-weighted and weighted methods—for computing the numbers of the interacting neighbors (Supplemental Figure 5). The non-weighted method merely counts the number of interacting neighbors, assuming that different types of interactions (PPIs, PDIs, and GIs) are equally important in pertaining a gene as a functional hub. In contrast, the weighted method computes the sum of the scores for the interactions linking a gene to its neighbors ('Methods' section). The scores represent the importance of interaction types, assuming that different types of interactions have their due importance. In this study, we used the non-weighted method for computing the numbers of the neighbors (see the 'Discussion' section for comparison of these two methods).

Using the non-weighted method, we first computed the number of the first or second neighbors for individual genes in each cluster and then calculated the significance of the numbers of the first (P_{1st}) or second (P_{2nd}) neighbors. Potential key regulators in each cluster were selected as the genes with significant numbers of the first or second neighbors ($P_{1st} < 0.1$ and $P_{2nd} < 0.1$, respectively; Figure 4A). Furthermore, the clusters with many key regulators can represent the major modes of interplays. Thus, iNID then identified these major clusters. To this end, for each cluster, iNID provides a cluster *P*-value (P^C) that represents whether the cluster has a significant number of key regulators. Among the eight clusters in Figure 3C, we selected the four major clusters (C1, C2, C3, and C4) indicated by asterisk in Figure 4A, with significant numbers of potential key regulators ($P^C_{1st} < 0.01$ or $P^C_{2nd} < 0.01$ in Figure 4A; 'Methods' section).

We then examined whether these four clusters (C1–C4) representing the major modes of interplays are associated with cellular processes regulated by auxin, BR, and/or blue light (Figure 4B) using 'Related biological processes' in iNID (e.g. magenta arrow in Figure 3C). Among the four clusters, C1 includes the largest number of the genes involved in hypocotyl elongation-related processes ('Growth' and 'Plant-type cell wall organization') and the processes related to auxin, BR, and light ('Response to light stimulus', 'Response to BR stimulus', and 'Response to auxin stimulus'). The results, together with the cluster *P*-values, indicate that C1 represents most strongly the interplay among auxin, BR, and blue light. The cluster navigator (green arrows in Figures 3C and 4A) shows that C1 includes both early and late responsive genes up-regulated by auxin and BR, but down-regulated by blue light (Figure 4C).

Based on these results, we focused on C1 representing antagonistic interplays between blue light and two phytohormones. We then examined the key regulators selected from the genes in C1. Combining the five and eight key regulators with $P_{1st} < 0.1$ and $P_{2nd} < 0.1$, respectively ('Key regulators' for C1 in Figure 4A), C1 included a total of eight unique key regulators (BME3, AT5G05090, AT1G21910 (DREB26), TEM1, ANAC029, PKS4, IAA3/SHY2, and AT1G79700; Figure 4D). Among the eight potential key regulators, two (SHY2 and PKS4) were previously shown to play their roles in auxin–BR–light signaling (Supplemental Table 2) (Colon-Carmona et al., 2000; Tian et al., 2002, 2003; Weijers et al., 2005; Schepens et al., 2008). *SHY2* negatively regulates auxin signaling (Tian et al., 2002) and is also involved in light signaling, as indicated by its interaction with PHYA and PHYB (Colon-Carmona et al., 2000; Tian et al., 2003). The suppression of the hypocotyl elongation phenotype of *phyB* mutant in the *shy2-2* gain-of-function mutants also indicates the involvement of *SHY2* in light signaling (Reed et al., 1998). Another regulator, PKS4, a member of the PHYTOCHROME KINASE SUBSTRATE (PKS)

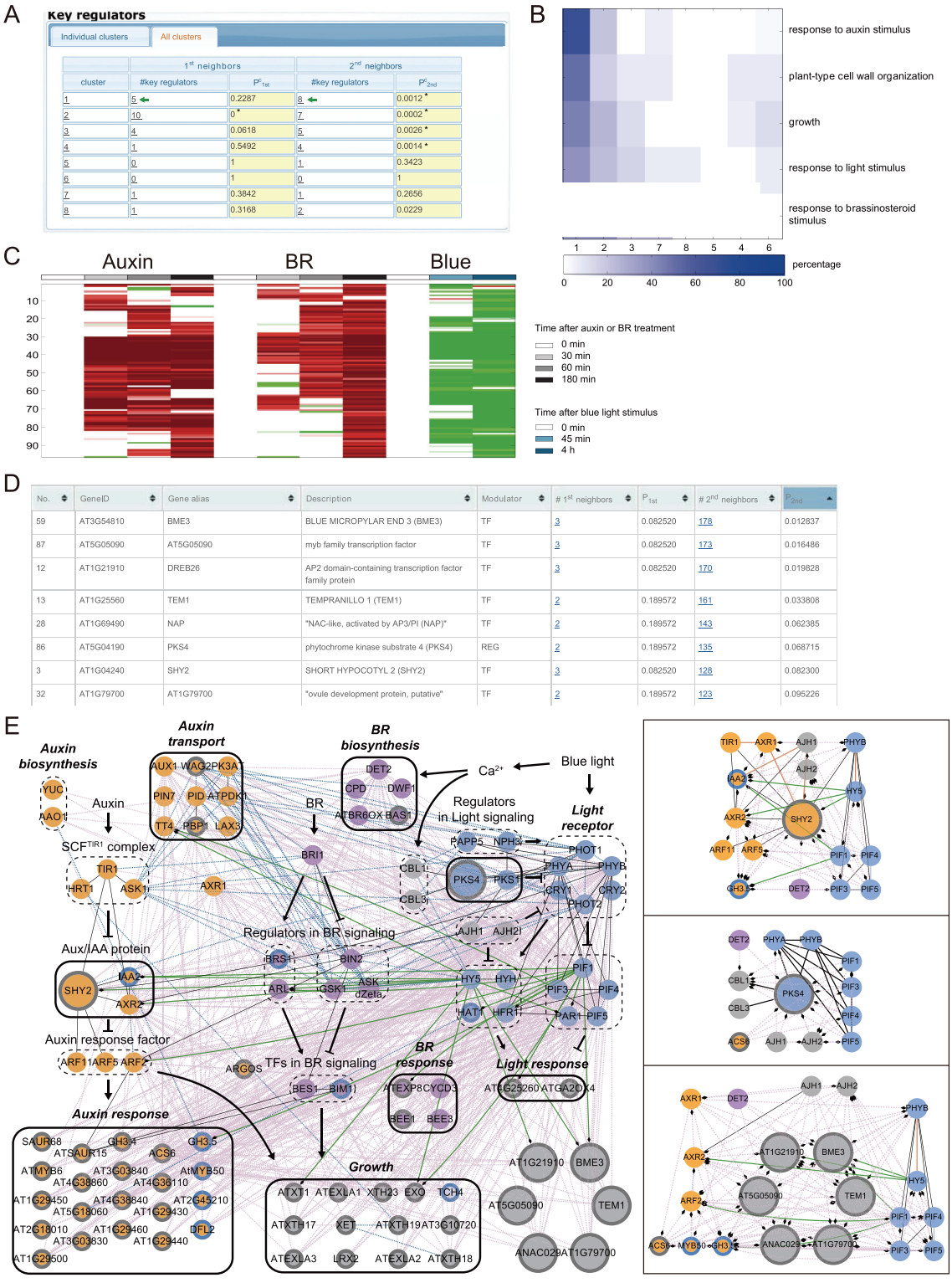

Figure 4. Identification of Key Regulators and a Network Model for the Auxin–BR–Blue Light Interplays.

(A) The number of potential key regulators identified from the genes in each cluster. P^{C}_{1st} and P^{C}_{2nd} represent cluster *P*-values that have the numbers of key regulators based on the first and second neighbors, respectively ('Methods' section). 'All clusters' tab above the table indicates that the total 281 DEGs in all the eight clusters were used to count the first and second neighbors during the selection of key regulators.

(B) GO biological processes (GOBPs) represented by the genes in each cluster. iNID first selected GOBPs represented by the genes in all clusters with enrichment P ≤ 0.1 (default cut-off in DAVID) and then displayed the fractions of the genes annotated with the selected GOBPs in individual clusters (Supplemental Figure 4C). Color bar, gradient of the fraction.

family, suppresses *PhyA*- and *PhyB*-dependent inhibition of hypocotyl elongation, which is also regulated by auxin and BR (Schepens et al., 2008). *BME3* (Liu et al., 2005), *TEM1* (Castillejo and Pelaz, 2008), and *ANAC029* (Guo and Gan, 2006) modulate germination, flowering, and senescence, respectively, which can be regulated by auxin, BR, and/or light (Jiao et al., 2007; Depuydt and Hardtke, 2011).

Development of a Network Model Delineating the Auxin–BR–Blue Light Interplay

To understand how the eight key regulators selected from C1 collectively contribute to the auxin–BR–blue light interplay, iNID also provides a network model (Figure 4E) that delineates the auxin–BR–light interplay. The network model was generated using the interactions between the eight key regulators and the genes in C1 based on the interactome data in iNID (see the 'Methods' section for further detail). iNID visualizes the network model using Cytoscape (Smoot et al., 2011). The network model included 104 nodes (e.g. genes or proteins) that comprise the eight key regulators (large nodes in Figure 4E), 37 genes in C1 (nodes with black boundaries in Figure 4E), and 59 of their first neighbors involved in the auxin, BR, or light pathways. These nodes were first grouped into auxin, BR, and light pathways (orange, magenta, and blue nodes, respectively) according to the pathway models (Figure 2B). The nodes belonging to each pathway were further sub-grouped into modules based on their functions (e.g. receptors, signaling molecules, transporters, and responsive genes). For example, the auxin pathway includes the modules associated with 'Auxin transport', 'Aux/IAA protein' (repressors in auxin signaling), and 'Auxin response'.

The network model revealed potential functional roles of the identified key regulators in the interplay among auxin, BR, and blue light, together with their known roles in each pathway. For example, SHY2, a selected key regulator, negatively regulates auxin signaling (Tian et al., 2002) together with Aux/IAA proteins, leading to suppression of expression of auxin-responsive genes. SHY2 also interacts with PHYB, a light receptor, and its promoter activity is regulated by HY5, a major downstream TF in light signaling (1st box in Figure 4E). Moreover, genetic associations (Supplementary Data 2) showed that the expression of *SHY2* could be affected by several factors involved in auxin (*GH3.5*), BR (*DET2*), and light (*PIF1/3/4/5*) signaling (pink dashed lines in 1st box in Figure 4E). PKS4, another selected regulator, negatively regulates light signaling in hypocotyl growth orientation (Schepens et al., 2008). It also interacts with Ca^{2+} sensors, CBL1/3 (2nd box in Figure 4E). Ca^{2+} signaling plays a critical role in BR biosynthesis via a calmodulin-binding protein DWF1 (Du and Poovaiah, 2005) and in inhibition of hypocotyl growth by blue light (Folta et al., 2003). The genetic associations further showed that the expression of *PKS4* could be affected by several factors involved in auxin (*ACS6*), BR (*DET2*), and light (*PIF1/3/4/5*) signaling. In addition, the network model suggests novel functions of the key regulators in the interplay. Genetic associations of the five potential key regulators (DREB26, BME3, AT5G05090, ANAC029, and TEM1) indicate that their expression can be affected by several factors in auxin (*AXR1/2*, *ARF2*, *ACS6*, *ATMYB50*, or *GH3.5*), BR (*DET2*), and light (*PhyB* or *PIF1/3/4/5*) signaling (3rd box in Figure 4E). Taken together, the network model provides the hypotheses for roles of the eight potential regulators in auxin–BR–blue light interplays.

Experimental Validation of the Involvement of BME3 and TEM1 in the Auxin–BR–Blue Light Interplay

To experimentally test the involvement of the identified key regulators in auxin–BR–blue light interplays, among the eight potential key regulators, we selected *BME3* and *TEM1* for which there has been no evidence supporting their direct associations with the auxin–BR–light interplay. Using RT–PCR analysis, we first confirmed the differential expression of *BME3* and *TEM1* detected by microarray analysis after treatments of auxin, BR, and light (i.e. increased expression by auxin or BR and decreased expression by light stimulus) (Figure 5A). To test the involvements of *BME3* and *TEM1* in the interplays of auxin, BR, and light, we then examined the responses of their T-DNA insertion knockout mutants (*bme3* and *tem1*) to auxin, BR, and light. The mutants showed altered expression of the auxin (*SAUR27*), BR (*BAS1*), and light-responsive (*PKS4* and *GA2OX6*) genes included in C1 after treatments of auxin, BR, and light (Figure 5B and 5C). These data indicate

(C) The heat map showing the expression patterns of the genes in cluster 1 (C1). The expression changes of each gene (row) in 30, 60, and 180 min after treatments of auxin and BR, and in 45 min and 4 h after the exposure to blue light are shown in columns. Red and green, up- and down-regulation in time points, respectively, under the corresponding conditions. Color bar, gradient of $\log_2$-fold-changes.
(D) The potential key regulators identified from the genes in C1. For each regulator, the table shows the numbers of the first and second neighbors among the 281 shared DEGs in auxin, BR, and blue light-treated conditions, as well as P_{1st} and P_{2nd}.
(E) A network model for the interplay. Node colors represent involvement of the genes in auxin (orange), BR (purple), or light (blue) pathways, and the process (Figure 4B) associated with the interplay (gray). Node boundary colors represent whether the corresponding genes were included in C1 (black) or the 281 shared DEGs (blue). Large nodes indicate the selected key regulators from the genes in C1. A module (solid black box) was named by the corresponding GOBPs. Three sub-networks (right panels) were generated to clearly show the interactions of the selected eight regulators (SHY2, PKS4, and six unknown regulators, respectively). Black lines, PPIs; orange lines, GIs; green lines, PDIs; dashed gray lines, predicted PPIs; dashed blue lines, predicted functional interactions; dashed pink lines, genetic associations identified from gene expression profiles of mutants. Target genes in PDIs and genes affected by mutations in genetic associations from gene expression profiles were denoted by diamond heads in these edges. The activation (arrow) and inhibition (inhibition symbol) information between the nodes (e.g. DEGs or key regulators) was obtained from previous literatures of the nodes.

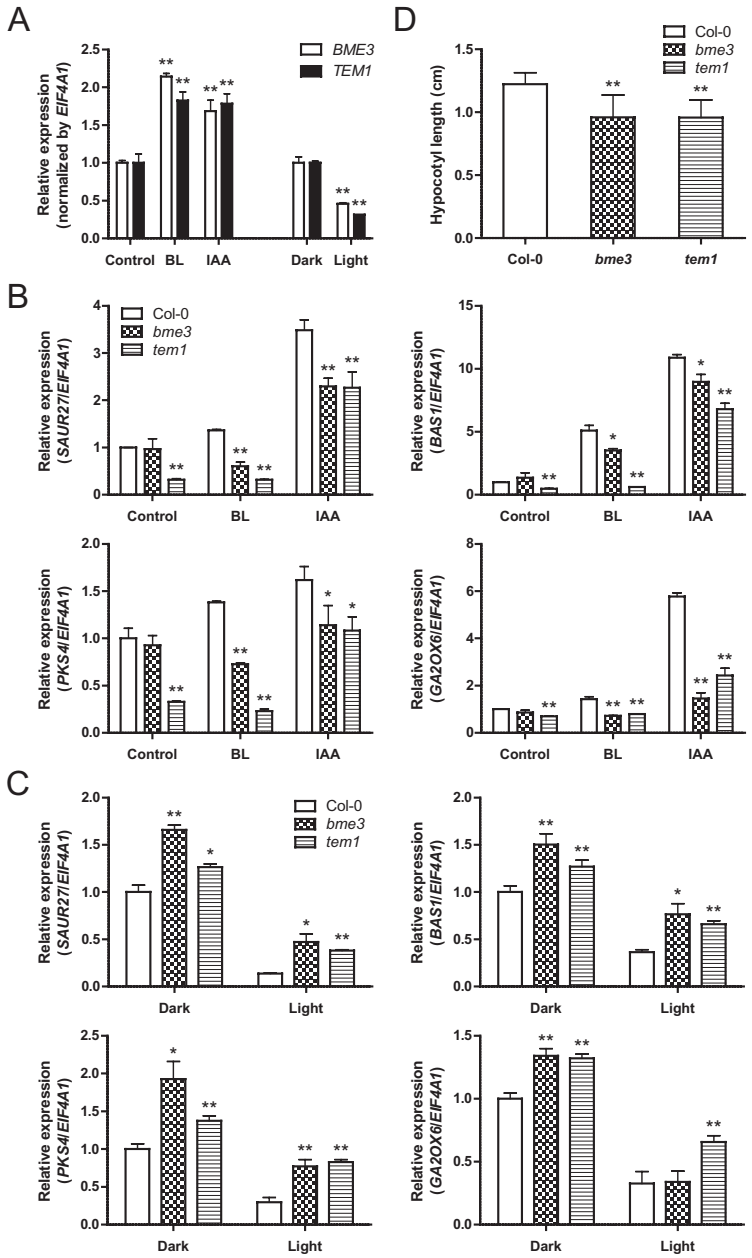

Figure 5. Experimental Validation of Two Selected Key Regulators, BME3 and TEM1, in the Auxin–BR–Light Interplay.

(A) Differential expressions of *BME3* and *TEM1* after treatments of indole-3-acetic acid (IAA), brassinolide (BL), and light determined by quantitative RT–PCR. The expression levels of the genes were normalized by that of eukaryotic translation initiation factor 4A-1 (*EIF4A1*) gene. The normalized expression levels of non-treated (control) or dark conditions were set to 1, and relative expression levels of *BME3* and *TEM1* in indicated conditions were plotted ($n = 3$).

(B, C) The relative expression levels of auxin- (*SAUR27*), BR- (*BAS1*), and light-responsive (*PKS4*, and *GA2OX6*) genes in C1 after treatments of IAA and BL (B), and after light stimulus (C) in wild-type (Col-0), *bme3*, and *tem1*. The normalized expression levels of non-treated (control; (B)) or dark conditions (C) in wild-type were set to 1, and relative expression levels of the four genes in indicated genotypes and conditions are plotted ($n = 3$).

(D) The hypocotyl lengths of 5-day-old seedlings ($n = 45$~51) of Col-0, *bme3*, and *tem1* grown under the dark conditions. Error bars indicate standard deviations. ** $P < 0.01$; * $P < 0.05$ (Student's *t*-test).

that BME3 and TEM1 regulate the expression of the auxin, BR, and light-responsive genes represented in the network model describing the auxin–BR–light interplay. Furthermore, in these mutants, we examined the changes in hypocotyl elongation that is regulated by auxin, BR, and/or light and also was strongly represented by the genes in C1 (Figure 4B). The results revealed that the deletion of *BME3* and *TEM1* led to suppressed hypocotyl elongation in dark-grown conditions (Figure 5D). Taken together, all these data indicate that BME3 and TEM1 function as novel regulators that contribute to

the auxin–BR–light interplay through the regulation of gene expression and physiology related to the interplay.

Comparison of iNID with Previous Tools in Identification of Key Regulators and Network Models for Auxin–BR–Blue Light Interplays

We summarized above a dozen of tools for analysis of transcriptome data and network analysis (Supplemental Table 1). Among them, only VirtualPlant provides a tool ('Network statistics') that computes the numbers of interacting neighbors of the genes in the resulting network. These numbers of neighbors can be used to identify key regulators as in iNID (Figure 4A). Unlike iNID, however, 'Network statistics' in VirtualPlant provides no statistical significance of the number of neighbors (*P*-values in Figure 4D), and thus an arbitrary cut-off for the number of neighbors should be used to select key regulators. For the comparison of key regulators that can be selected from the 96 genes in C1 by iNID (Figure 4D) and VirtualPlant, we first calculated the numbers of the first and second neighbors of the 96 genes in the network using 'Network statistics' in VirtualPlant. Then, the four key regulators (SHY2, At5g50570, At5g67060, and At1g77640) (Supplemental Figure 6A) were selected with the cut-offs used for the selection in iNID (i.e. the numbers of first and second neighbors = 3 and 123, corresponding to $P_{1st} < 0.1$ and $P_{2nd} < 0.1$, respectively; Figure 4D). Among the four key regulators, only SHY2 with the largest number of neighbors (Supplemental Figure 6A) is shared with the eight key regulators (Figure 4D) identified by iNID. The discrepancy in the key regulators selected by VirtualPlant and iNID can be due to the difference in the interactome data sets between VirtualPlant and iNID.

Next, we compared a network model generated from iNID with those (Supplemental Figure 6) generated by three representative tools—GeneMANIA, ATTED-II, and VirtualPlant—using the 96 genes in C1 and their first neighbors based on various interactome data (Supplemental Table 1). iNID assigns pathway information (auxin, BR, and light pathways) to nodes according to the pathway models, facilitating functional organization of the nodes for enhanced interpretation of a network model (Supplemental Figure 6B). Unlike iNID, however, GeneMANIA, ATTED-II, and VirtualPlant provided no pathway information for nodes. Instead, GeneMANIA provides information about gene ontology biological processes (GOBPs) represented by the nodes. ATTED-II provides subcellular localization information of the nodes predicted by Target P (Emanuelsson et al., 2000) and WoLF PSORT (Horton et al., 2007). For the comparison of the networks, we analyzed how well the network models from individual tools represented auxin, BR, and light pathways by counting the numbers of the genes related to the three pathways. For this analysis, we used GOBPs for the nodes in network models generated from ATTED-II (Supplemental Figure 6C), GeneMANIA (Supplemental Figure 6D), and VirtualPlant (Supplemental Figure 6E). The comparison revealed that the network model generated from iNID most significantly represented all auxin, BR, and light pathways (Supplemental Figure 6F). All these data showed that, compared to the three representative tools, iNID provides the most useful tool to identify key regulators and network models for the auxin–BR–light interplays.

Case Study 2: Interplays between Hormones and Biotic Stresses

Phytohormones function as essential internal factors that control not only developmental processes, but also responses to biotic stress (Bari and Jones, 2009; Robert-Seilaniantz et al., 2011). Plants interact with a number of pathogens during their growth and development. Phytohormones have different roles in the plant–pathogen interaction, depending on species of pathogens (biotroph or necrotroph), activities of pathogen effectors, or infection sites (Ton et al., 2009). SA is considered to be involved in response to biotrophs, while JA and ET are involved in response to necrotrophs (Glazebrook, 2005). ABA suppresses callose deposition after the treatment of the bacterial flagellin Flg22 (Clay et al., 2009), but induces the callose deposition after the infection of fungal necrotrophs (Ton and Mauch-Mani, 2004). However, previous studies have focused mainly on relationships between individual phytohormones and pathogens. To better understand cooperative actions of phytohormones against multiple pathogens, a systemic approach for investigating the interplays between phytohormones and pathogens is required. Thus, in this second case study, we applied iNID to systematically identify key regulators and network models for the interplays between phytohormones and biotic stresses.

We first selected gene expression data sets collected after treatments of eight phytohormones (ABA, auxin, BR, CK, ET, GA, JA, and SA) and nine pathogens (*Psm* ES4326, *Psm* ES4326 avrRpt2, *Pst* DC3000, *Pst* avrRpm1, *Pst* DC3000 hrcC$^-$, *Psp*, *B. cinerea*, *P. infestans*, and *E. orontii*) in iNID (Supplemental Figure 7). To identify the modes of the interplays under these 17 conditions, among the two clustering methods in iNID, we used the NMF clustering method (Kim et al., 2011) (red arrow in Supplemental Figure 7) that effectively identifies clusters of the genes showing differential expression patterns (DEPs) across a large number of conditions (see the 'Methods' section for further detail). Using the NMF clustering, we first identified 30 clusters (Supplemental Figure 8). Among them, we then selected eight clusters (C1 to C8 in Figure 6A, red arrows in Supplemental Figures 8 and 9) associated with the interplays between phytohormones and biotic stresses with DEPs under at least one of phytohormone-treated conditions and one of the pathogen-infected conditions. C1, C2, C3, and C6, among the eight clusters, showed expression changes by SA and the pathogens, indicating potential interplays between SA and biotic stress. In particular, C1 and C3 showed down-regulation by both SA and the eight pathogens, whereas C2 showed the opposite expression pattern. Interestingly, C6 exhibited strong activation in systemic tissues by the two pathogens, *Psm* ES4326 and *Psm* avrRpt2, but relatively weak

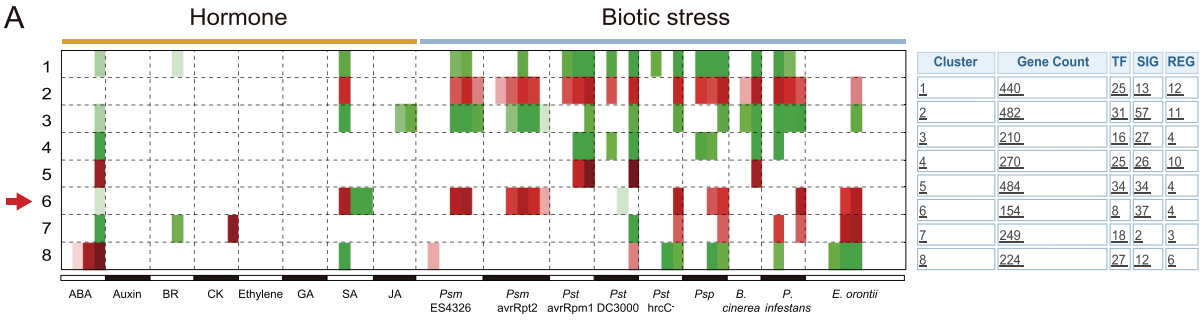

Cluster	Gene Count	TF	SIG	REG
1	440	25	13	12
2	482	31	57	11
3	210	16	27	4
4	270	25	26	10
5	484	34	34	4
6	154	8	37	4
7	249	18	2	3
8	224	27	12	6

B

Key regulators

Individual clusters | All clusters

	1st neighbors		2nd neighbors	
cluster	#key regulators	P^{c}_{1st}	#key regulators	P^{c}_{2nd}
1	1	0.9065	1	0.7869
2	7	0.0319	7	0.0001 *
3	2	0.3614	2	0.3245
4	5	0.0214	1	0.4019
5	1	0.9354	1	0.7587
6	17	1.51E-17 *	15	7.9E-14 *
7	5	2.6629E-6 *	7	3.0E-10 *
8	7	0.0002 *	2	0.1053

C

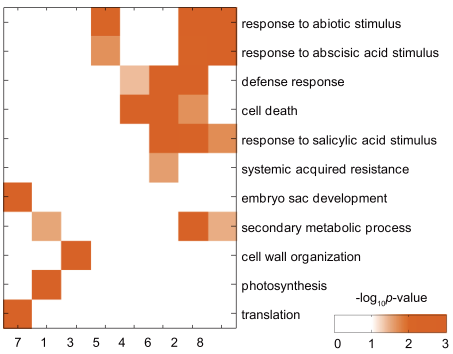

D

Gene ID	Gene alias	Description	#1st neighbors	P_{1st}	#2nd neighbors	P_{2nd}
AT1G66880	AT1G66880	serine/threonine protein kinase family protein	33	0.0035	94	0.002
AT1G35710	AT1G35710	leucine-rich repeat transmembrane protein kinase, putative	29	0.0041	86	0.0039
AT4G04500	AT4G04500	cystein-rich receptor-like protein kinase	28	0.0044	88	0.0033
AT2G32680	ATRLP23	Receptor Like Protein 23 (AtRLP23)	28	0.0044	81	0.0059
AT3G11010	ATRLP34	Receptor Like Protein 34 (AtRLP34)	27	0.0046	82	0.0055
AT1G34750	AT1G34750	protein phosphatase 2C, putative / PP2C, putative	26	0.0052	80	0.0068
AT3G25010	ATRLP41	Receptor Like Protein 41 (AtRLP41)	26	0.0052	76	0.0096
AT2G31880	AT2G31880	leucine-rich repeat transmembrane protein kinase, putative	25	0.0061	90	0.0027
AT1G08450	CRT3	CALRETICULIN 3 (CRT3)	24	0.0066	77	0.0087
AT4G08850	AT4G08850	leucine-rich repeat transmembrane protein kinase	23	0.007	88	0.0033
AT2G13790	BKK1	SOMATIC EMBRYOGENESIS RECEPTOR-LIKE KINASE 4 (SERK4)	22	0.0075	84	0.0045
AT5G60900	RLK1	RECEPTOR-LIKE PROTEIN KINASE 1 (RLK1)	22	0.0075	73	0.0189
AT1G21250	WAK1	CELL WALL-ASSOCIATED KINASE (WAK1)	21	0.0081	72	0.0196
AT4G18250	AT4G18250	receptor serine/threonine kinase, putative	19	0.0091	87	0.0036
AT3G48090	EDS1	enhanced disease susceptibility 1 (EDS1)	19	0.0091	86	0.0039
AT4G23220	CRK14	cystein-rich receptor-like protein kinase	18	0.0096	82	0.0055
AT4G24190	HSP90.7	SHEPHERD (SHD)	18	0.0096	61	0.0321
AT4G09570	CPK4	CPK4	16	0.0109	81	0.0059

E

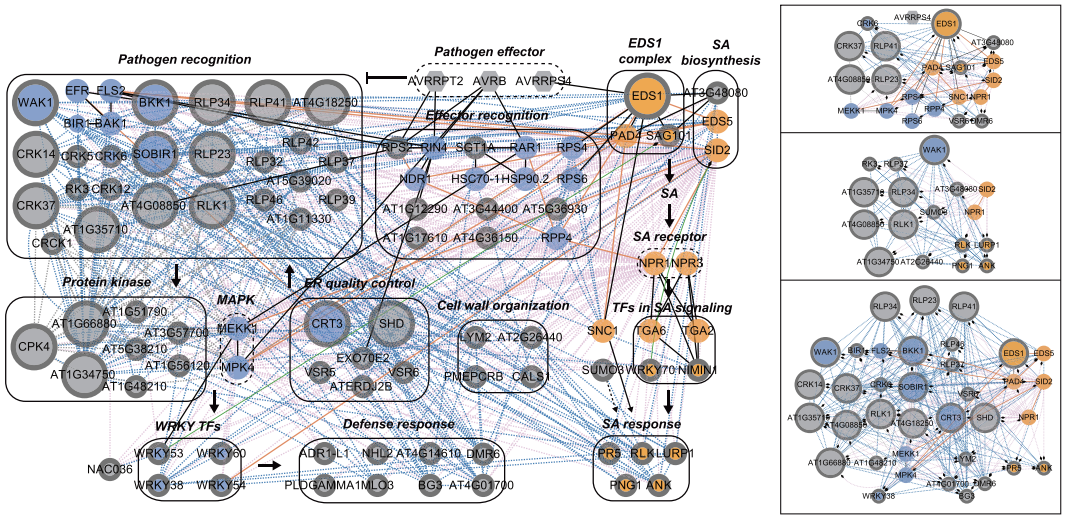

Figure 6. Interplays among Phytohormones and Biotic Stresses.

(A) The NMF result showing interplay-related expression patterns (rows) over time under phytohormone- and pathogen-treated conditions (denoted by labels in *x*-axis and dotted lines). Red and green, up- and down-regulation under the corresponding conditions, respectively. The numbers of the genes (also regulators) showing the expression patterns are summarized in the table. In each column, the boxes indicated by dotted lines showed temporal expression changes over time in the corresponding data set.

activation in local tissues by the four pathogens (*Pst* hrcC⁻, *Psp*, *P. infestans*, and *E. orontii*) compared to the activation shown in C2. Also, C6 showed no response to the other three pathogens (*Pst* avrRpm1, *Pst* DC3000, and *B. cinerea*) in local tissues. On the other hand, C4, C5, C7, and C8 showed expression changes by ABA and the pathogens, indicating potential interplays between the abiotic stress phytohormone, ABA, and biotic stress.

Among the eight clusters representing different modes of the interplays between pathogens and phytohormones, we selected C2, C6, C7, and C8 with significant numbers ($P^C_{1st} < 0.01$ or $P^C_{2nd} < 0.01$) of potential key regulators for the interplays (Figure 6B). GOBP enrichment analysis (Figure 6C) revealed that C2, C6, and C8, compared to C7, were strongly associated with both phytohormone responses ('Response to salicylic acid stimulus' and 'Response to abscisic acid stimulus') and biotic stress-related processes ('Defense response', 'Systemic acquired resistance', and 'Cell death'). Interestingly, C6 was associated with systemic acquired resistance (Figure 6C). Based on the cluster *P*-values and GO analysis, among the four clusters (C2, C6, C7, and C8), we first analyzed the genes in C6 to identify potential key regulators and network models for the interplay between SA and biotic stress involving systemic acquired resistance.

The Interplay between SA and Biotic Stress

Combining the 17 and 15 key regulators with $P_{1st} < 0.01$ and $P_{2nd} < 0.01$, respectively ('Key regulators' for C6 in Figure 6B), we selected a total of 18 unique key regulators (Figure 6D) from the genes in C6. Known functional roles of the 18 selected regulators in defense responses and/or SA signaling are summarized in Supplemental Table 3 (Clarke et al., 2001; Feys et al., 2001; He et al., 2007; Cabrera et al., 2008; Gao et al., 2009; Li et al., 2009; Bhattacharjee et al., 2011; Heidrich et al., 2011). Five of 18 were shown to be involved in SA and defense responses. For example, EDS1 is involved in R-gene-mediated effector-triggered immunity (ETI) (Feys et al., 2001; Heidrich et al., 2011), as well as SA biosynthesis (Feys et al., 2001) and signaling (Clarke et al., 2001). Ten were predicted to be related to SA and defense response (Heyndrickx and Vandepoele, 2012), including three receptor-like proteins (RLPs; AT3G11010, AT2G32680, and AT3G25010) and two leucine-rich repeat (LRR) transmembrane protein kinases (AT1G35710 and AT4G08850) whose family proteins are involved in pathogen recognition (Antolin-Llovera et al., 2012; Greeff et al., 2012). The remaining three had no function previously reported in association with SA and defense response.

To understand how the 18 potential key regulators can contribute to the interplay (Figure 6E), we generated a network model with 98 nodes including 18 key regulators (large nodes), 56 genes in C6 (nodes with black boundaries), and 24 first neighbors of the genes in C6. The 98 nodes were then arranged into SA and defense signaling pathways (orange and blue nodes, respectively) according to the pathway models in iNID (Figure 2B). The nodes in each pathway were further sub-grouped into modules based on their functions. SA signaling pathway included 'EDS1 complex', 'SA biosynthesis', 'TFs in SA signaling', and 'SA response' modules. Defense signaling pathway included 'Pathogen recognition' (pathogen-associated molecular pattern (PAMP) receptors (WAK1, BIR1, and BKK1), LRR transmembrane proteins (SOBIR1, AT1G35170, and AT1G07650), and RLPs and cysteine-rich RLP kinases (CRKs)), 'Effector recognition' (R-genes (RPS2 and putative R-genes) and R gene-mediated resistance related gene (SGT1A)), 'ER quality control' (CRT3, SHD, ATERDJ2B, EXO70E2, VSR5, and VSR6), 'WRKY TFs' (WRKY38/53/54/60), 'Protein kinase' (CPK4, AT5G38210, AT3G57700, AT1G66880, AT1G56120, AT1G51790, AT1G48210, and AT1G34750), and 'Cell wall organization' modules.

The network model revealed potential associations of the selected regulators with the interplays between SA and biotic stress. First, the network model supported known functional roles of the selected regulators in the interplay between SA and biotic stress. A selected regulator EDS1 recognizes pathogen effector, AvrRps4 (Heidrich et al., 2011), and propagates the defense signal by forming complexes with PAD4 and SAG101 (Zhu et al., 2011) (1st box in Figure 6E). The interactions of EDS1 with RPS4, RPS6, PAD4, SAG101, AT3G48080, and RLKs (CRK6, CRK37, AT4G08850, RLP23, and RLP41), as well as its genetic associations with *MPK4* and *RPP4* in defense signaling and *SID2* and *NPR1* in SA signaling, collectively supported the known role of EDS1 in the interplay between SA and defense responses. Second, the network model also revealed novel functions of the regulators in the interplays between SA and biotic stress, which were known to

(B) The numbers of selected key regulators and their cluster *P*-values (P^C_{1st} and P^C_{2nd}) in individual clusters. 'Individual clusters' tab above the table indicates that only the genes in C6, unlike the genes in all clusters in case study 1 (Figure 4A), were used to count the first and second neighbors during the selection of key regulators.

(C) GOBPs represented by the genes in individual clusters.

(D) Potential key regulators for the interplay between SA and biotic stress, as well as the numbers of their first and second neighbors and *P*-values (P_{1st} and P_{2nd}).

(E) A network model for the SA–biotic stress interplay. Node colors indicate the genes involved in SA (orange) and pathogen-related (blue) signaling and responses. The black boundary color represents that the corresponding genes were included in C6. Large nodes indicate the 18 potential key regulators mediating the interplay. Three sub-networks (right panels) were generated to clearly show the interactions of the selected regulators (EDS1, WAK1, and RLPs, respectively). Black lines, PPIs; orange lines, GIs; green lines, PDIs; dashed gray lines, predicted PPIs; dashed blue lines, functional interactions; dashed pink lines, genetic associations identified from gene expression profiles of mutants. See the legend of Figure 4E for diamond heads, activation, and inhibition symbols.

be involved in only either SA or defense signaling. WAK1 was known to be involved in defense response as a receptor of cell wall fragments released during pathogen invasion (Cabrera et al., 2008). The interactions of WAK1 with the components involved in SA biosynthesis (*SID2*), SA receptors (*NPR1*), and SA responses (*ANK*, *PNG1*, *LURP1*, and *RLK*) indicated its potential roles in SA signaling (2nd box in Figure 6E). Finally, the network model revealed that several selected regulators with no known function related to SA or defense response showed dense interactions with both SA and defense responses. For example, RLP23/34/41 closely interact with the components involved in SA-, defense-related signaling and responses (3rd box in Figure 6E).

The Interplay between ABA and Biotic Stress

In addition to the SA–biotic stress interplays, the NMF clustering (Figure 6A) also suggested the interplays among ABA and several pathogens. Among the four selected clusters (C2, C6, C7, and C8) with $P^{C}_{1st} < 0.01$ or $P^{C}_{2nd} < 0.01$ (Figure 6B), C8 showed up-regulation by ABA and down-regulation by the four pathogens (*Pst* hrcC^{-}, *Psp*, and *P. infestans*, and *E. orontii*), whereas C7 did the opposite expression pattern, implying the negative relationship between ABA and the responses to these pathogens. The GOBP enrichment analysis also revealed that, compared to C7, C8 is more strongly associated with ABA-related processes, such as 'Response to abiotic stimulus', 'Response to abscisic acid stimulus', and 'Secondary metabolic process' (Figure 6C).

Based on these results, we focused on C8 to understand an antagonistic interplay between ABA and biotic stress. Combining the seven and two key regulators with $P_{1st} < 0.01$ and $P_{2nd} < 0.01$, respectively ('Key regulators' for C6 in Figure 6B), we then identified a total of eight unique key regulators from the genes in C8 (Supplemental Figure 10A). Seven out of them have been reported to be involved in ABA, abiotic stress, or defense pathways (Supplemental Table 4) (Kurkela and Franck, 1990; Abe et al., 2003; Lorenzo et al., 2004; Kanwischer et al., 2005; Maeda et al., 2006; Sattler et al., 2006; Dombrecht et al., 2007; Novillo et al., 2007; Wang and Hua, 2009; Wang et al., 2011; Valdes et al., 2012). For example, MYC2, a MYC-related TF, functions as a signaling mediator between ABA and JA/ET-dependent defense pathways (Ton et al., 2009; Robert-Seilaniantz et al., 2011). MYC2 induces ABA-responsive genes (Abe et al., 2003) and also acts as a negative regulator of JA/ET-dependent defense response (Dombrecht et al., 2007).

We then generated a network model with 121 nodes including the eight key regulators, 74 genes in C8, and their 39 first neighbors (Supplemental Figure 10B). The nodes were then arranged into ABA (orange nodes) and JA/ET-dependent (blue and magenta nodes) defense signaling pathways according to the pathway models in iNID (Figure 2B) and then were further sub-grouped into modules in each pathway based on their functions. ABA signaling pathway included 'Protein Phosphatase 2C (PP2C)', 'SnRK', 'downstream TFs in ABA signaling', and 'Response to abiotic stress' modules. JA/ET-dependent defense signaling pathways included 'JAZ repressor', 'TFs in ET signaling', 'Defense response', and 'Wound response' modules.

As in the network model for SA–biotic stress interplays (Figure 6E), this network model also shows known and novel associations of the selected regulators with ABA–biotic stress interplays. First, the network model supported known functional roles of the selected regulators in the ABA–biotic stress interplays. MYC2 and its homologs (MYC3 and MYC4) densely interact with the negative regulators of JA signaling in 'JAZ repressor' module (1st box in Supplemental Figure 10B). *MYC2* had further genetic associations with ABI1 and downstream TFs (*ABI5*, *MYB32/91*, and *HB-7/12*) in ABA signaling. Second, the network model also revealed novel functions of the regulators in ABA–biotic stress interplays, which were known to be involved in only either ABA or defense signaling. For example, *KIN1*, a marker gene of ABA and cold stress (Kurkela and Franck, 1990), had dense functional interactions with the molecules in 'Response to abiotic stress' and 'Defense response' modules (2nd box in Supplemental Figure 10B). Interestingly, another selected regulator CCA1, a core component in the circadian network (Wang and Tobin, 1998; Pruneda-Paz and Kay, 2010), had genetic associations with the molecules in ABA and JA/ET-dependent defense signaling pathways (Supplemental Figure 11), suggesting that the circadian clock can modulate functions of ABA and biotic stress. In support of this network-driven hypothesis, recently, *CCA1* was identified as an essential regulator for temporal control of the expression of defense-related genes (Wang et al., 2011).

DISCUSSION

Identification of key regulators and network models for interplays among various IEFs is essential to understand coordinated controls in plant development by the IEFs. Although several methods have been developed, they still lack tools that can perform the integrative analysis to identify key regulators and network models for the interplays among IEFs. In this study, we developed an analytical framework, called iNID, for effectively identifying key regulators and biological networks for the interplays. The applications of iNID to the three interplay problems (auxin–BR–light, SA–biotic stress, and ABA–biotic stress interplays) revealed several known regulators mediating the interplays and also potential novel regulators, as well as network models delineating how these known and potential regulators collectively act to mediate the interplays among the IEFs. As demonstrated in these case studies, iNID can be also applied to combinations of IEFs for which the mechanisms underlying the interplays among the IEFs are unknown. The resulting potential novel regulators and network models provide hypotheses that can be further tested by detailed functional experiments, thus serving as the

bases for enhancing understanding of the interplays among the IEFs.

iNID includes the data sets generated from plants at various developmental stages of *Arabidopsis* genotypes (Table 1). The analysis of interplay-related expression patterns and regulators using the data sets generated from different developmental stages may lead to inappropriate biological context and misinterpretation of the data. To partially resolve this problem, iNID normalizes probe intensities across gene expression profiles in each data set using the same GCRMA normalization method ('Methods' section). This normalization would reduce variations coming from different developmental stages and experimental conditions used in different laboratories. In addition to the normalization of probe intensities, to further reduce the issue of the variations, iNID normalizes $\log_2$-fold-changes of individual data sets by the quantile normalization method ('Methods' section) before identifying interplay-related expression patterns using the NMF method. In the first case study, to understand the interplays among auxin, BR, and blue light, we used the data sets generated at the same seedling stage after treatments of auxin, BR, and blue light. However, in the second case study, we used the data sets generated at two different developmental stages (seedling stage for hormone data sets and adult stage for biotic stress data sets) to understand the interplays between hormones and biotic stresses. The variations between seedling and adult stages may lead to false positive interplay-related expression patterns and regulators. To avoid this issue, we focused on the expression pattern reflecting the interaction between hormones (i.e. SA or ABA) and biotic stresses for which supporting evidence exists.

To select key regulators based on the degrees, iNID provides an option for the use of non-weighted or weighted edges to compute P_{1st} and P_{2nd} and for the computation of betweenness centralities (BWCs) (Supplemental Figure 5). In the two case studies, 8 (auxin–BR–blue light interplay), 13 (SA–biotic stress interplay), and 7 key regulators (ABA–biotic stress interplay) were selected using weighted edges (Supplemental Figure 12A–12C, respectively). Comparison of the key regulators selected using non-weighted (Figures 4D, 6D, and Supplemental Figure 10A) and weighted edges (Supplemental Figure 12A–12C) revealed that the same eight key regulators were selected for the auxin–BR–blue light interplay even when the weighted edges were used. However, five (WAK1, CRT3, BKK1, CRK14, and HSP90.7) and one (COR15) key regulators were not selected when the weighted edges were used. This indicates that they might be less important key regulators than other key regulators selected using both non-weighted and weighted edges. Interestingly, no additional key regulators were selected using the weighted edges for computing P_{1st} and P_{2nd}.

Han et al. (2004) suggested that party hubs act as local coordinators that link the components in a module, whereas date hubs act as global coordinators that mediate the interactions among the modules (Han et al., 2004). Agarwal et al. (2010) also proposed that BWC for each node, which is defined by the number of shortest paths from all nodes to all other nodes that pass through the node, can be used as a metric to determine party and date hubs (Agarwal et al., 2010). They further showed that date hubs had higher BWCs on average, compared to party hubs. Thus, iNID provides an option to calculate BWCs for the selected key regulators, as described in Agarwal et al. (2010), and *P*-values of the BWCs (Supplemental Figures 12 and 13). BWCs for the key regulators selected using non-weighted edges (Supplemental Figure 13A–13C) showed that no key regulators selected for the auxin–BR–blue light interplay had significant BWCs (i.e. $P_{BWC} > 0.05$ in Supplemental Figure 13A). In contrast, one (AT1G34750) and four (PIF4, CCA1, VTE1, and MYC2) key regulators selected for the SA– and ABA–biotic stress interplays, respectively, had significant BWCs ($P_{BWC} < 0.05$ in Supplemental Figure 13B and 13C). Thus, these five regulators can be considered as date hubs or global coordinators according to the guideline in Agarwal et al. (2010). Interestingly, the two key regulators (BME3 and TEM1) with $P_{BWC} > 0.05$ (Supplemental Figure 13A), which can be considered as party hubs or local coordinators, were experimentally verified to be involved in the auxin–BR–light interplay (Figure 5). These data suggest that these two party hubs can function as key regulators at least in the auxin–BR–light interplay investigated. All these data indicate that the edge weighting and BWC can provide complementary natures for selection of the key regulators, providing various aspects of potential key regulators for the interplays among IEFs.

The integrity of a network model can be judged through certain topological features. To understand the importance of the selected key regulators, it is important to examine how robust the network models are against the removal of the key regulators from the network models. To this end, we estimated the average shortest path lengths as removing the selected key regulators and the non-key regulators from the network model and then compared the average shortest path lengths after the removal of the key regulators and non-key regulators (Supplemental Figure 14). For this analysis, we used the average shortest path length as a metric to quantify the impact of deleting the nodes as previously described (Albert and Barabási, 2002). The results showed that the removal of the key regulators from the network models led to the increase in the average shortest path lengths of all the network models reconstructed for the three interplays investigated in this study. Moreover, the increase in the average shortest path length resulted from the removal of the key regulators was more apparent than that which was resulted from the removal of the non-key regulators (*P*-values from one-way ANOVA < 0.05). This indicates that the key regulators have higher impacts on the connectivity in the network models representing the interplays among the IEFs in the network models, compared to the non-key regulators in the

network models. Thus, these data confirmed the importance of the key regulators selected by P_{1st} and P_{2nd}.

Recently, NGS-based transcriptomic data, such as mRNA-seq data, have been accumulated. iNID provides the interface to upload users' own transcriptomic data. The interface takes *P*-values (or FDRs) and $\log_2$-fold-changes (Supplemental Figure 1B). Thus, *P*-values and $\log_2$-fold-changes for NGS-based transcriptomic data can be first computed using users' own tools and can be then imported to iNID using this interface. However, the scales of the *P*-values and $\log_2$-fold-changes can be different from those computed from microarray data. Using the quantile normalization method, iNID normalizes the $\log_2$-fold-changes from different NGS or microarray data to correct the variations in the scale between NGS and microarray data sets. Furthermore, the scale difference in the *P*-values between NGS and microarray data sets can be reduced by using the tool used to compute *P*-values in this study, which can be downloaded from the iNID website.

iNID is a web-based tool that has a broad spectrum of applicability and easy expandability. To increase the applicability, iNID provides an interface to upload users' own transcriptome data into iNID and to investigate the interplays between their IEFs and the 41 IEFs in iNID (Supplemental Figure 1B). Furthermore, users can investigate DEPs for a list of genes of users' interest and thus can select potential regulators associated with the interplay between IEFs being investigated (Supplemental Figure 1A). To achieve the expandability, iNID uses Cytoscape and its plug-ins for visualization and analyses of network models. When these tools are improved, iNID can incorporate immediately new functionalities of these tools. In addition, new transcriptome data sets, interactomes, and pathway information will be updated regularly to extend the resources in iNID. These aspects enable iNID to serve as a useful tool to enhance understanding of interplays among various IEFs during plant growth and development.

METHODS

Collection of Gene Expression Data Sets

We first obtained 41 time-course gene expression data sets collected after treatments of IEFs described in Table 1 from AtGenExpress (Kilian et al., 2007; Goda et al., 2008) and Arrayexpress (Parkinson et al., 2007). For each data set, the intensities of the probes were $\log_2$-transformed and then normalized using the GCRMA method (Wu et al., 2004). To determine whether a gene was expressed under a IEF-treated condition, the mixture of two Gaussian models, one for non-expressed (absent) probes and the other for expressed (present) probes, was fitted to the distribution of the normalized $\log_2$-intensity (Lee et al., 2010a; Kim et al., 2012). We considered a gene to be expressed if the normalized intensity of the gene was larger than a cut-off intensity in which the two Gaussian models meet in at least one sample. Among the expressed genes, we identified DEGs as described below. For each data set, both the normalized expression data and the absent/present calls were deposited into iNID.

Identification of Differentially Expressed Genes

To identify DEGs in each data set, we calculated the overall *P*-values by the following method previously reported (Hwang et al., 2005a; Chae et al., 2013): (1) *t*-statistic values and $\log_2$-median-differences between the normalized intensities in control and IEF-treated conditions in individual time points were calculated; (2) *t*-values (or $\log_2$-median-differences) at all the time points were summed by the trapezoidal method (Thomas et al., 2007); (3) an empirical distribution of the summed *t*-value (or $\log_2$-median-differences) was generated by randomly permuting all the samples in the data set; (4) for each probe set, an adjusted *P*-value of the summed *t*-value (or $\log_2$-median-differences) was computed using the corresponding empirical distribution; and (5) for each probe set, the adjusted *P*-values from the *t*-statistic values and $\log_2$-median-differences were combined into an adjusted overall *P* using Stouffer's method (Hwang et al., 2005b). DEGs are selected as the genes with adjusted overall $P <$ a user's specified cut-off value (e.g. 0.05 in case study 1). To remove potential false positives, we further selected DEGs with absolute $\log_2$-mediance-difference $\geq$ a user's specified threshold (e.g. 0.58, 1.5-fold-change in the original scale) at least one time point. iNID further provides FDRs of the overall *P*-values computed by Storey's method (Storey and Tibshirani, 2003). The FDRs can be used to select DEGs instead of the adjusted overall *P*-values used in this study. The MATLAB code for this analysis is provided through the iNID webpage (Supplemental Figure 1).

Identification of Genetic Associations from Mutant Microarray Data

To identify genetic associations from gene expression profiles of mutants, we first collected 389 data sets obtained from *Arabidopsis* mutants and their wild-types. In each data set, using the above methods, we then normalized the intensity data and identified the DEGs with overall $P < 0.05$ and absolute $\log_2$-mediance-difference ≥ 0.58. Finally, we generated genetic associations between the DEGs and the gene mutated in the data set. The lists of the data sets and the interactions are provided in Supplemental Data 2.

Clustering of Differential Expression Patterns

iNID provides two methods ('Clustering' box in Figure 4A) for clustering the genes showing differential expression: (1) 'Pattern analysis' and (2) NMF method. First, for a set of genes, pattern analysis classifies the genes in each data set into three groups: up-regulated ($P < 0.05$; $\log_2$-fold-change > 0.58 at least one time point), down-regulated ($P < 0.05$; $\log_2$-fold-change < -0.58 at least one time point), or not changed ($P > 0.05$ or $-0.58 < \log_2$-fold-change < 0.58) genes. It then clusters the genes into all possible combinations of the DEPs

in the selected data sets. Although this pattern analysis is simple and fast, the use of the deterministic *P*-value and fold-change cut-offs could result in false negative errors when the fold-changes less than the cut-off can be truly significant. To partially remedy this problem, we employed the NMF method that identifies the DEPs (clusters) across the selected data sets as previously described in detail (Kim et al., 2011). Among several NMF variants, we used the orthogonal NMF (ONMF). In case study 2, we identified 30 DEPs after 30 applications of ONMF and 1000 iterations of each ONMF (Kim et al., 2011). Before the ONMF clustering, the $\log_2$-fold-changes in individual data were normalized to correct the difference in the distribution of the $\log_2$-fold-changes arising from different developmental stages and types of the used tissues and different experimental conditions using the quantile normalization method (Bolstad et al., 2003). For each DEP associated with the interplay, we selected the interplay-related genes with $P \leq 0.02$. The *P*-value indicates the significance that a gene shows the corresponding DEP. Its cut-off was determined by examining whether the selected genes actually showed the DEP for multiple cut-off values between 0.05 and 0.01. Compared to pattern analysis using the deterministic cut-offs, the NMF method focuses on the DEPs across all individual data sets during the clustering, which allows us to select the genes with marginal fold-changes in some data sets when they showed clear DEPs in the other data sets. As previously demonstrated (Kim et al., 2011), for a large number of data sets, the NMF method tends to effectively cluster the genes. In contrast, for a small number of data sets, the simple pattern analysis produces similar results to those obtained from the NMF method.

Identification of Potential Key Regulators Mediating Interplays

iNID selects key regulators from the genes with regulatory activities (e.g. TF or kinase activity) according to GO molecular functions (GOMFs) in each interplay-related cluster. For each regulator, using the interactome data in iNID, we first computed the number of first and second neighbors among the genes in a set of DEGs selected for the analysis from the Venn diagram (Figure 3B) or the interplay-related patterns (Figure 6A) (e.g. 281 shared DEGs in case study 1 and 154 and 224 genes in C6 and C8, respectively, in case study 2). Two methods, the non-weighted and weighted methods, were used for computing the numbers of the interacting neighbors (Supplemental Figure 5): the non-weighted method merely counts the number of interacting neighbors using non-weighted edges, whereas the weighted method computes the sum of the scores for the interactions linking a gene to its neighbors using weighted edges. Then, two distributions of the counts of the first and second neighbors were generated using the numbers of first and second neighbors of all the genes (22 746 genes in ATH1 microarray) in the same domain, respectively. For the numbers of first and second neighbors of each regulator in the cluster, two *P*-values (P_{1st} and P_{2nd}) were estimated using the corresponding distributions. Finally, key regulators are selected as the genes with one of the two *P*-values less than a given threshold (e.g. $P < 0.01$). Also, to assess whether the selected key regulators can serve as party or date hubs, BWCs were evaluated for all the genes in a selected cluster using the NetworkX Python package (Hagberg et al., 2008). To calculate the significance (*P*-values) of the BWC, we randomly sampled the same number of genes with the selected DEGs 2000 times, computed the BWCs for the randomly sampled genes, and estimated an empirical distribution of the BWCs. Using the distribution, *P*-values of the observed BWCs for the selected key regulators were estimated by the one-tailed test.

Confidence Score of the Interactions

Edges can have their due importance in pertaining a node as a regulatory hub. We estimated the confidence of the interactions in iNID using the method previously used in the STRING database (von Mering et al., 2005). We first defined three true positive sets of PPIs (PPI_{true}), PDIs (PDI_{true}), and GIs (GI_{true}) using the curated interactomes in iNID, respectively. These true positive interactions are similar to the interactions in the KEGG database that STRING used as true positive interactions. Using the true positive sets, we then evaluated the scores for PPIs, PDIs, and GIs in each source of the interactions (e.g. AtORFeome2.0, PPIN-1, Intact, etc.; see reference in Figure 2A) as follows: (1) we counted overlapping nodes between the nodes with true positive PPIs (PPI_{true}) and with all the PPIs in the source (PPI_{ref}); (2) we then counted the PPIs including the overlapping nodes in the true positive PPI_{true} (N_{true_PPI}) and the source (N_{ref_PPI}); (3) we estimated the score (S_{PPI}) as N_{ref_PPI} divided by N_{true_PPI}; and (4) the same procedure was done to estimate S_{PDI} and S_{GI} using PDI_{true}–PDI_{ref} and GI_{true}–GI_{ref}, respectively. This procedure is similar to that performed to estimate the score using the interactions in the KEGG database and in the individual sources. For the sources providing the predicted interactions (e.g. Aranet and Interactome 2.0), it is not clear which types of interactions the predicted interactions refer to. Therefore, we computed a representative score for the predicted interactions by combining the scores (S_{PPI}, S_{PDI}, and S_{GI}) estimated for PPIs, PDIs, and GIs using the naive Bayesian algorithm as previously described in STRING (von Mering et al., 2005). These scores were used as weights of the edges in each source.

Identification of Major Clusters Related to Interplays

iNID selects major interplay-related clusters with significant numbers of key regulators. Key regulators from the genes in each cluster are first chosen by the method described above. For key regulators in each cluster, iNID calculates a cluster *P*-value (P^c) using Fisher's exact test using the genes in the cluster and all the genes in ATH1 microarray. Then, iNID selects major interplay-related clusters as the ones with ($P^c_{1st} < 0.01$ or $P^c_{2nd} < 0.01$).

Reconstruction of Network Models for Interplays

iNID provides a 'Network modeling' tool for reconstruction of a network model delineating the interplay. For an interplay-related cluster (e.g. C1 in case study 1 and C6 and C8 in case study 2), we first selected the genes including the key regulators in the cluster using the 'Cluster navigator' page. To understand their functions and find their associated pathways, we then expanded the network models by incorporating the first neighbors of the selected genes (blue arrow in Supplemental Figure 15). The 'Network modeling' tool visualizes the resulting network using Cytoscape. Among the genes in the initial network, we then chose (1) the key regulators and (2) the genes involved in the pathways related to the IEFs and the processes represented by the interplay-related genes (e.g. 'response to light stimulus' in case study 1 in Figure 4B). Finally, the nodes in the resulting network were arranged according to the pathway models and the cellular processes in which the nodes are involved. Furthermore, the known genes involved in the pathways related to the IEFs (e.g. auxin, BR, and light in case study 1; ABA, SA, and defense in case study 2) could be added using the 'Add a list of genes' tool (green box in Supplemental Figure 15).

Validation of the Involvement of Key Regulators in the Auxin–BR–Light Interplay

To test the response to auxin and BR, seedlings of wild-type (Col-0), *bme3* (SALK_131396), and *tem1* (SALK_097513) were grown in 0.5 Murashige and Skoog (Duchefa Biochemie) liquid medium (pH 5.6) containing 1.2% sucrose for 5 d at 23°C under continuous light. The seedlings were then treated with 1 μM of indole-3-acetic acid or 10 nM of brassinolide. After 3 h, they were immediately frozen in liquid nitrogen. To test the response to light stimulus and measure the hypocotyl length of dark-grown seedlings, seedlings of wild-type, *bme3*, and *tem1* were grown on 0.5 Murashige and Skoog medium (pH 5.6) containing 1.2% sucrose and 0.8% agar type-M (Sigma) for 5 d under the dark. The seedlings were then exposed to light for 4 h and immediately frozen in liquid nitrogen. The hypocotyl length was measured from digital photo of the seedlings using Scion Image software. To determine the expression levels of auxin, BR, and light-responsive genes, total RNAs were isolated from the seedlings using Trizol reagent (Invitrogen). cDNAs were synthesized from 1 μg of the RNAs using ImProm-II first-strand synthesis system (Promega Corp.) with an oligo(dT)18 primer. The quantitative real-time RT–PCR was performed using SYBR Premix Ex Taq (TaKaRa Bio Inc.) and analyzed by ABI StepOnePlus (Applied Biosystems). The analysis was performed using three biological replicates. The measurement was normalized using the expression level of the gene encoding *eukaryotic translation initiation factor 4A-1* (*EIF4A1*) gene (AT3G13920). Primers used in real-time RT–PCR are listed in Supplemental Table 5.

SUPPLEMENTARY DATA

Supplementary Data are available at *Molecular Plant Online.*

FUNDING

This study was supported by grants from the Next-Generation BioGreen21 Program (PJ009072, PJ009516), Institute for Basic Science (CA1308), Proteogenomics program, POSCO Research Fund (Project NO. 2013Y008), the ABC of Global Frontier projects (ABC-2010–0029720), and Mid-career Researcher Program (2012R1A2A2A02014387). No conflict of interest declared.

REFERENCES

Abe, H., Urao, T., Ito, T., Seki, M., Shinozaki, K., and Yamaguchi-Shinozaki, K. (2003). *Arabidopsis* AtMYC2 (bHLH) and AtMYB2 (MYB) function as transcriptional activators in abscisic acid signaling. Plant Cell. **15**, 63–78.

Agarwal, S., Deane, C.M., Porter, M.A., and Jones, N.S. (2010). Revisiting date and party hubs: novel approaches to role assignment in protein interaction networks. PLoS Computational Biology. **6**, e1000817.

Alabadi, D., and Blazquez, M.A. (2009). Molecular interactions between light and hormone signaling to control plant growth. Plant Mol. Biol. **69**, 409–417.

Albert, R., and Barabási, A.-L. (2002). Statistical mechanics of complex networks. Rev. Mod. Phys. **74**, 47.

Antolin-Llovera, M., Ried, M.K., Binder, A., and Parniske, M. (2012). Receptor kinase signaling pathways in plant–microbe interactions. Annu. Rev. Phytopathol. **50**, 451–473.

Bader, G.D., Betel, D., and Hogue, C.W. (2003). BIND: the Biomolecular Interaction Network Database. Nucleic Acids Res. **31**, 248–250.

Barabasi, A.L., and Oltvai, Z.N. (2004). Network biology: understanding the cell's functional organization. Nat. Rev. Genet. **5**, 101–113.

Barabasi, A.L., Gulbahce, N., and Loscalzo, J. (2011). Network medicine: a network-based approach to human disease. Nat. Rev. Genet. **12**, 56–68.

Bari, R., and Jones, J.D. (2009). Role of plant hormones in plant defence responses. Plant Mol. Biol. **69**, 473–488.

Bhattacharjee, S., Halane, M.K., Kim, S.H., and Gassmann, W. (2011). Pathogen effectors target *Arabidopsis* EDS1 and alter its interactions with immune regulators. Science. **334**, 1405–1408.

Bolstad, B.M., Irizarry, R.A., Astrand, M., and Speed, T.P. (2003). A comparison of normalization methods for high density oligonucleotide array data based on variance and bias. Bioinformatics. **19**, 185–193.

Brandao, M.M., Dantas, L.L., and Silva-Filho, M.C. (2009). AtPIN: *Arabidopsis thaliana* protein interaction network. BMC Bioinformatics. **10**, 454.

Braun, P., Carvunis, A.R., Charloteaux, B., Dreze, M., Ecker, J.R., Hill, D.E., Roth, F.P., Vidal, M., Galli, M., Balumuri, P., et al. (2011). Evidence for network evolution in an *Arabidopsis* interactome map. Science. **333**, 601–607.

Cabrera, J.C., Boland, A., Messiaen, J., Cambier, P., and Van Cutsem, P. (2008). Egg box conformation of oligogalacturonides: the time-dependent stabilization of the elicitor-active conformation increases its biological activity. Glycobiology. **18**, 473–482.

Castillejo, C., and Pelaz, S. (2008). The balance between CONSTANS and TEMPRANILLO activities determines FT expression to trigger flowering. Curr. Biol. **18**, 1338–1343.

Chae, S., Ahn, B.Y., Byun, K., Cho, Y.M., Yu, M.-H., Lee, B., Hwang, D., and Park, K.S. (2013). A systems approach for decoding mitochondrial retrograde signaling pathways. Science Signaling. **6**, rs4.

Chan, Z. (2012). Expression profiling of ABA pathway transcripts indicates crosstalk between abiotic and biotic stress responses in *Arabidopsis*. Genomics. **100**, 110–115.

Chen, Y.A., Wen, Y.C., and Chang, W.C. (2012). AtPAN: an integrated system for reconstructing transcriptional regulatory networks in *Arabidopsis thaliana*. BMC Genomics. **13**, 85.

Clarke, J.D., Aarts, N., Feys, B.J., Dong, X., and Parker, J.E. (2001). Constitutive disease resistance requires EDS1 in the *Arabidopsis* mutants cpr1 and cpr6 and is partially EDS1-dependent in cpr5. Plant J. **26**, 409–420.

Clay, N.K., Adio, A.M., Denoux, C., Jander, G., and Ausubel, F.M. (2009). Glucosinolate metabolites required for an *Arabidopsis* innate immune response. Science. **323**, 95–101.

Colon-Carmona, A., Chen, D.L., Yeh, K.C., and Abel, S. (2000). Aux/IAA proteins are phosphorylated by phytochrome *in vitro*. Plant Physiol. **124**, 1728–1738.

Cui, J., Li, P., Li, G., Xu, F., Zhao, C., Li, Y., Yang, Z., Wang, G., Yu, Q., and Shi, T. (2008). AtPID: *Arabidopsis thaliana* protein interactome database: an integrative platform for plant systems biology. Nucleic Acids Res. **36**, D999–D1008.

De Bodt, S., Carvajal, D., Hollunder, J., Van den Cruyce, J., Movahedi, S., and Inze, D. (2010). CORNET: a user-friendly tool for data mining and integration. Plant Physiol. **152**, 1167–1179.

Depuydt, S., and Hardtke, C.S. (2011). Hormone signalling crosstalk in plant growth regulation. Curr. Biol. **21**, R365–R373.

Devarajan, K. (2008). Nonnegative matrix factorization: an analytical and interpretive tool in computational biology. PLoS Computational Biology. **4**, e1000029.

Dombrecht, B., Xue, G.P., Sprague, S.J., Kirkegaard, J.A., Ross, J.J., Reid, J.B., Fitt, G.P., Sewelam, N., Schenk, P.M., Manners, J.M., et al. (2007). MYC2 differentially modulates diverse jasmonate-dependent functions in *Arabidopsis*. Plant Cell. **19**, 2225–2245.

Du, L., and Poovaiah, B.W. (2005). Ca2+/calmodulin is critical for brassinosteroid biosynthesis and plant growth. Nature. **437**, 741–745.

Emanuelsson, O., Nielsen, H., Brunak, S., and von Heijne, G. (2000). Predicting subcellular localization of proteins based on their N-terminal amino acid sequence. J. Mol. Biol. **300**, 1005–1016.

Feys, B.J., Moisan, L.J., Newman, M.A., and Parker, J.E. (2001). Direct interaction between the *Arabidopsis* disease resistance signaling proteins, EDS1 and PAD4. EMBO J. **20**, 5400–5411.

Folta, K.M., Lieg, E.J., Durham, T., and Spalding, E.P. (2003). Primary inhibition of hypocotyl growth and phototropism depend differently on phototropin-mediated increases in cytoplasmic calcium induced by blue light. Plant Physiol. **133**, 1464–1470.

Gao, M., Wang, X., Wang, D., Xu, F., Ding, X., Zhang, Z., Bi, D., Cheng, Y.T., Chen, S., Li, X., et al. (2009). Regulation of cell death and innate immunity by two receptor-like kinases in *Arabidopsis*. Cell Host & Microbe. **6**, 34–44.

Geisler-Lee, J., O'Toole, N., Ammar, R., Provart, N.J., Millar, A.H., and Geisler, M. (2007). A predicted interactome for *Arabidopsis*. Plant Physiol. **145**, 317–329.

Giorgi, F.M., Del Fabbro, C., and Licausi, F. (2013). Comparative study of RNA-seq- and Microarray-derived coexpression networks in *Arabidopsis thaliana*. Bioinformatics. **29**, 717–724.

Glazebrook, J. (2005). Contrasting mechanisms of defense against biotrophic and necrotrophic pathogens. Annu. Rev. Phytopathol. **43**, 205–227.

Goda, H., Sasaki, E., Akiyama, K., Maruyama-Nakashita, A., Nakabayashi, K., Li, W., Ogawa, M., Yamauchi, Y., Preston, J., Aoki, K., et al. (2008). The AtGenExpress hormone and chemical treatment data set: experimental design, data evaluation, model data analysis and data access. Plant J. **55**, 526–542.

Greeff, C., Roux, M., Mundy, J., and Petersen, M. (2012). Receptor-like kinase complexes in plant innate immunity. Frontiers in Plant Science. **3**, 209.

Guo, Y., and Gan, S. (2006). AtNAP, a NAC family transcription factor, has an important role in leaf senescence. Plant J. **46**, 601–612.

Gutierrez, R.A., Lejay, L.V., Dean, A., Chiaromonte, F., Shasha, D.E., and Coruzzi, G.M. (2007). Qualitative network models and genome-wide expression data define carbon/nitrogen-responsive molecular machines in *Arabidopsis*. Genome Biol. **8**, R7.

Hagberg, A., Swart, P., and Schult, D. (2008). Exploring Network Structure, Dynamics, and Function Using NetworkX (Los Alamos, NM: Los Alamos National Laboratory (LANL)).

Han, J.D., Bertin, N., Hao, T., Goldberg, D.S., Berriz, G.F., Zhang, L.V., Dupuy, D., Walhout, A.J., Cusick, M.E., Roth, F.P., et al. (2004). Evidence for dynamically organized modularity in the yeast protein–protein interaction network. Nature. **430**, 88–93.

Hardtke, C.S., Dorcey, E., Osmont, K.S., and Sibout, R. (2007). Phytohormone collaboration: zooming in on auxin–brassinosteroid interactions. Trends Cell Biol. **17**, 485–492.

He, K., Gou, X., Yuan, T., Lin, H., Asami, T., Yoshida, S., Russell, S.D., and Li, J. (2007). BAK1 and BKK1 regulate brassinosteroid-dependent growth and brassinosteroid-independent cell-death pathways. Curr. Biol. **17**, 1109–1115.

Heidrich, K., Wirthmueller, L., Tasset, C., Pouzet, C., Deslandes, L., and Parker, J.E. (2011). *Arabidopsis* EDS1 connects pathogen effector recognition to cell compartment-specific immune responses. Science. **334**, 1401–1404.

Heyndrickx, K.S., and Vandepoele, K. (2012). Systematic identification of functional plant modules through the integration of complementary data sources. Plant Physiol. **159**, 884–901.

Hisamatsu, T., and King, R.W. (2008). The nature of floral signals in *Arabidopsis*. II. Roles for FLOWERING LOCUS T (FT) and gibberellin. J. Exp. Bot. **59**, 3821–3829.

Horton, P., Park, K.J., Obayashi, T., Fujita, N., Harada, H., Adams-Collier, C.J., and Nakai, K. (2007). WoLF PSORT: protein localization predictor. Nucleic Acids Res. **35**, W585–W587.

Hruz, T., Laule, O., Szabo, G., Wessendorp, F., Bleuler, S., Oertle, L., Widmayer, P., Gruissem, W., and Zimmermann, P. (2008). Genevestigator v3: a reference expression database for the

meta-analysis of transcriptomes. Advances in Bioinformatics. **2008**, 420747.

Hwang, D., Lee, I.Y., Yoo, H., Gehlenborg, N., Cho, J.H., Petritis, B., Baxter, D., Pitstick, R., Young, R., Spicer, D., et al. (2009). A systems approach to prion disease. Molecular Systems Biology. **5**, 252.

Hwang, D., Rust, A.G., Ramsey, S., Smith, J.J., Leslie, D.M., Weston, A.D., De Atauri, P., Aitchison, J.D., Hood, L., and Siegel, A.F. (2005a). A data integration methodology for systems biology. Proc. Natl Acad. Sci. U S A. **102**, 17296–17301.

Hwang, D., Smith, J.J., Leslie, D.M., Weston, A.D., Rust, A.G., Ramsey, S., de Atauri, P., Siegel, A.F., Bolouri, H., Aitchison, J.D., et al. (2005b). A data integration methodology for systems biology: experimental verification. Proc. Natl Acad. Sci. U S A. **102**, 17302–17307.

Jiang, Z., Liu, X., Peng, Z., Wan, Y., Ji, Y., He, W., Wan, W., Luo, J., and Guo, H. (2011). AHD2.0: an update version of Arabidopsis Hormone Database for plant systematic studies. Nucleic Acids Res. **39**, D1123–D1129.

Jiao, Y., Lau, O.S., and Deng, X.W. (2007). Light-regulated transcriptional networks in higher plants. Nat. Rev. Genet. **8**, 217–230.

Kanehisa, M., Goto, S., Hattori, M., Aoki-Kinoshita, K.F., Itoh, M., Kawashima, S., Katayama, T., Araki, M., and Hirakawa, M. (2006). From genomics to chemical genomics: new developments in KEGG. Nucleic Acids Res. **34**, D354–D357.

Kanwischer, M., Porfirova, S., Bergmuller, E., and Dormann, P. (2005). Alterations in tocopherol cyclase activity in transgenic and mutant plants of *Arabidopsis* affect tocopherol content, tocopherol composition, and oxidative stress. Plant Physiol. **137**, 713–723.

Katari, M.S., Nowicki, S.D., Aceituno, F.F., Nero, D., Kelfer, J., Thompson, L.P., Cabello, J.M., Davidson, R.S., Goldberg, A.P., Shasha, D.E., et al. (2010). VirtualPlant: a software platform to support systems biology research. Plant Physiol. **152**, 500–515.

Kerrien, S., Alam-Faruque, Y., Aranda, B., Bancarz, I., Bridge, A., Derow, C., Dimmer, E., Feuermann, M., Friedrichsen, A., Huntley, R., et al. (2007). IntAct—open source resource for molecular interaction data. Nucleic Acids Res. **35**, D561–D565.

Kilian, J., Whitehead, D., Horak, J., Wanke, D., Weinl, S., Batistic, O., D'Angelo, C., Bornberg-Bauer, E., Kudla, J., and Harter, K. (2007). The AtGenExpress global stress expression data set: protocols, evaluation and model data analysis of UV-B light, drought and cold stress responses. Plant J. **50**, 347–363.

Kim, K., Choi, D., Kim, S.M., Kwak, D.Y., Choi, J., Lee, S., Lee, B.C., Hwang, D., and Hwang, I. (2012). A systems approach for identifying resistance factors to Rice stripe virus. Mol. Plant Microbe Interact. **25**, 534–545.

Kim, Y., Kim, T.K., Kim, Y., Yoo, J., You, S., Lee, I., Carlson, G., Hood, L., Choi, S., and Hwang, D. (2011). Principal network analysis: identification of subnetworks representing major dynamics using gene expression data. Bioinformatics. **27**, 391–398.

Kurkela, S., and Franck, M. (1990). Cloning and characterization of a cold- and ABA-inducible *Arabidopsis* gene. Plant Mol. Biol. **15**, 137–144.

Lamesch, P., Berardini, T.Z., Li, D., Swarbreck, D., Wilks, C., Sasidharan, R., Muller, R., Dreher, K., Alexander, D.L., Garcia-Hernandez, M., et al. (2012). The *Arabidopsis* Information Resource (TAIR): improved gene annotation and new tools. Nucleic Acids Res. **40**, D1202–D1210.

Lau, O.S., and Deng, X.W. (2010). Plant hormone signaling lightens up: integrators of light and hormones. Curr. Opin. Plant Biol. **13**, 571–577.

Lee, H.J., Suk, J.E., Patrick, C., Bae, E.J., Cho, J.H., Rho, S., Hwang, D., Masliah, E., and Lee, S.J. (2010a). Direct transfer of alpha-synuclein from neuron to astroglia causes inflammatory responses in synucleinopathies. J. Biol. Chem. **285**, 9262–9272.

Lee, I., Ambaru, B., Thakkar, P., Marcotte, E.M., and Rhee, S.Y. (2010b). Rational association of genes with traits using a genome-scale gene network for *Arabidopsis thaliana*. Nat. Biotechnol. **28**, 149–156.

Li, J., Zhao-Hui, C., Batoux, M., Nekrasov, V., Roux, M., Chinchilla, D., Zipfel, C., and Jones, J.D. (2009). Specific ER quality control components required for biogenesis of the plant innate immune receptor EFR. Proc. Natl Acad. Sci. U S A. **106**, 15973–15978.

Liu, P.P., Koizuka, N., Martin, R.C., and Nonogaki, H. (2005). The BME3 (Blue Micropylar End 3) GATA zinc finger transcription factor is a positive regulator of *Arabidopsis* seed germination. Plant J. **44**, 960–971.

Lorenzo, O., Chico, J.M., Sanchez-Serrano, J.J., and Solano, R. (2004). JASMONATE-INSENSITIVE1 encodes a MYC transcription factor essential to discriminate between different jasmonate-regulated defense responses in *Arabidopsis*. Plant Cell. **16**, 1938–1950.

Luo, X.M., Lin, W.H., Zhu, S., Zhu, J.Y., Sun, Y., Fan, X.Y., Cheng, M., Hao, Y., Oh, E., Tian, M., et al. (2010). Integration of light- and brassinosteroid-signaling pathways by a GATA transcription factor in *Arabidopsis*. Dev. Cell. **19**, 872–883.

Maeda, H., Song, W., Sage, T.L., and DellaPenna, D. (2006). Tocopherols play a crucial role in low-temperature adaptation and Phloem loading in *Arabidopsis*. Plant Cell. **18**, 2710–2732.

Matys, V., Fricke, E., Geffers, R., Gossling, E., Haubrock, M., Hehl, R., Hornischer, K., Karas, D., Kel, A.E., Kel-Margoulis, O.V., et al. (2003). TRANSFAC: transcriptional regulation, from patterns to profiles. Nucleic Acids Res. **31**, 374–378.

Moon, J., Suh, S.S., Lee, H., Choi, K.R., Hong, C.B., Paek, N.C., Kim, S.G., and Lee, I. (2003). The SOC1 MADS-box gene integrates vernalization and gibberellin signals for flowering in *Arabidopsis*. Plant J. **35**, 613–623.

Mostafavi, S., Ray, D., Warde-Farley, D., Grouios, C., and Morris, Q. (2008). GeneMANIA: a real-time multiple association network integration algorithm for predicting gene function. Genome Biol. **9**, S4.

Mukhtar, M.S., Carvunis, A.R., Dreze, M., Epple, P., Steinbrenner, J., Moore, J., Tasan, M., Galli, M., Hao, T., Nishimura, M.T., et al. (2011). Independently evolved virulence effectors converge onto hubs in a plant immune system network. Science. **333**, 596–601.

Nemhauser, J.L., Hong, F., and Chory, J. (2006). Different plant hormones regulate similar processes through largely nonoverlapping transcriptional responses. Cell. **126**, 467–475.

Novillo, F., Medina, J., and Salinas, J. (2007). *Arabidopsis* CBF1 and CBF3 have a different function than CBF2 in cold acclimation and define different gene classes in the CBF regulon. Proc. Natl Acad. Sci. U S A. **104**, 21002–21007.

Obayashi, T., Kinoshita, K., Nakai, K., Shibaoka, M., Hayashi, S., Saeki, M., Shibata, D., Saito, K., and Ohta, H. (2007). ATTED-II: a database of co-expressed genes and cis elements for identifying co-regulated gene groups in *Arabidopsis*. Nucleic Acids Res. **35**, D863–D869.

Parkinson, H., Kapushesky, M., Shojatalab, M., Abeygunawardena, N., Coulson, R., Farne, A., Holloway, E., Kolesnykov, N., Lilja, P., Lukk, M., et al. (2007). ArrayExpress: a public database of microarray experiments and gene expression profiles. Nucleic Acids Res. **35**, D747–D750.

Pruneda-Paz, J.L., and Kay, S.A. (2010). An expanding universe of circadian networks in higher plants. Trends Plant Sci. **15**, 259–265.

Reed, J.W., Elumalai, R.P., and Chory, J. (1998). Suppressors of an *Arabidopsis thaliana* phyB mutation identify genes that control light signaling and hypocotyl elongation. Genetics. **148**, 1295–1310.

Robert-Seilaniantz, A., Grant, M., and Jones, J.D. (2011). Hormone crosstalk in plant disease and defense: more than just jasmonate–salicylate antagonism. Annu. Rev. Phytopathol. **49**, 317–343.

Sattler, S.E., Mene-Saffrane, L., Farmer, E.E., Krischke, M., Mueller, M.J., and DellaPenna, D. (2006). Nonenzymatic lipid peroxidation reprograms gene expression and activates defense markers in *Arabidopsis* tocopherol-deficient mutants. Plant Cell. **18**, 3706–3720.

Schepens, I., Boccalandro, H.E., Kami, C., Casal, J.J., and Fankhauser, C. (2008). PHYTOCHROME KINASE SUBSTRATE4 modulates phytochrome-mediated control of hypocotyl growth orientation. Plant Physiol. **147**, 661–671.

Smoot, M.E., Ono, K., Ruscheinski, J., Wang, P.L., and Ideker, T. (2011). Cytoscape 2.8: new features for data integration and network visualization. Bioinformatics. **27**, 431–432.

Srikanth, A., and Schmid, M. (2011). Regulation of flowering time: all roads lead to Rome. Cell Mol. Life Sci. **68**, 2013–2037.

Stark, C., Breitkreutz, B.J., Chatr-Aryamontri, A., Boucher, L., Oughtred, R., Livstone, M.S., Nixon, J., Van Auken, K., Wang, X., Shi, X., et al. (2011). The BioGRID Interaction Database: 2011 update. Nucleic Acids Res. **39**, D698–D704.

Steinhauser, D., Usadel, B., Luedemann, A., Thimm, O., and Kopka, J. (2004). CSB.DB: a comprehensive systems-biology database. Bioinformatics. **20**, 3647–3651.

Storey, J.D., and Tibshirani, R. (2003). Statistical significance for genomewide studies. Proc. Natl Acad. Sci. U S A. **100**, 9440–9445.

Thomas, R., Paredes, C.J., Mehrotra, S., Hatzimanikatis, V., and Papoutsakis, E.T. (2007). A model-based optimization framework for the inference of regulatory interactions using time-course DNA microarray expression data. BMC Bioinformatics. **8**, 228.

Tian, Q., Nagpal, P., and Reed, J.W. (2003). Regulation of *Arabidopsis* SHY2/IAA3 protein turnover. Plant J. **36**, 643–651.

Tian, Q., Uhlir, N.J., and Reed, J.W. (2002). *Arabidopsis* SHY2/IAA3 inhibits auxin-regulated gene expression. Plant Cell. **14**, 301–319.

Ton, J., and Mauch-Mani, B. (2004). Beta-amino-butyric acid-induced resistance against necrotrophic pathogens is based on ABA-dependent priming for callose. Plant J. **38**, 119–130.

Ton, J., Flors, V., and Mauch-Mani, B. (2009). The multifaceted role of ABA in disease resistance. Trends Plant Sci. **14**, 310–317.

Toufighi, K., Brady, S.M., Austin, R., Ly, E., and Provart, N.J. (2005). The Botany Array Resource: e-Northerns, Expression Angling, and promoter analyses. Plant J. **43**, 153–163.

Valdes, A.E., Overnas, E., Johansson, H., Rada-Iglesias, A., and Engstrom, P. (2012). The homeodomain-leucine zipper (HD-Zip) class I transcription factors ATHB7 and ATHB12 modulate abscisic acid signalling by regulating protein phosphatase 2C and abscisic acid receptor gene activities. Plant Mol. Biol. **80**, 405–418.

van Leeuwen, H., Kliebenstein, D.J., West, M.A., Kim, K., van Poecke, R., Katagiri, F., Michelmore, R.W., Doerge, R.W., and St Clair, D.A. (2007). Natural variation among *Arabidopsis thaliana* accessions for transcriptome response to exogenous salicylic acid. Plant Cell. **19**, 2099–2110.

Vert, G., Walcher, C.L., Chory, J., and Nemhauser, J.L. (2008). Integration of auxin and brassinosteroid pathways by Auxin Response Factor 2. Proc. Natl Acad. Sci. U S A. **105**, 9829–9834.

von Mering, C., Jensen, L.J., Snel, B., Hooper, S.D., Krupp, M., Foglierini, M., Jouffre, N., Huynen, M.A., and Bork, P. (2005). STRING: known and predicted protein–protein associations, integrated and transferred across organisms. Nucleic Acids Res. **33**, D433–D437.

Wan, Y., Jasik, J., Wang, L., Hao, H., Volkmann, D., Menzel, D., Mancuso, S., Baluska, F., and Lin, J. (2012). The signal transducer NPH3 integrates the phototropin1 photosensor with PIN2-based polar auxin transport in *Arabidopsis* root phototropism. Plant Cell. **24**, 551–565.

Wang, W., Barnaby, J.Y., Tada, Y., Li, H., Tor, M., Caldelari, D., Lee, D.U., Fu, X.D., and Dong, X. (2011). Timing of plant immune responses by a central circadian regulator. Nature. **470**, 110–114.

Wang, Y., and Hua, J. (2009). A moderate decrease in temperature induces COR15a expression through the CBF signaling cascade and enhances freezing tolerance. Plant J. **60**, 340–349.

Wang, Z.Y., and Tobin, E.M. (1998). Constitutive expression of the CIRCADIAN CLOCK ASSOCIATED 1 (CCA1) gene disrupts circadian rhythms and suppresses its own expression. Cell. **93**, 1207–1217.

Weijers, D., Benkova, E., Jager, K.E., Schlereth, A., Hamann, T., Kientz, M., Wilmoth, J.C., Reed, J.W., and Jurgens, G. (2005). Developmental specificity of auxin response by pairs of ARF and Aux/IAA transcriptional regulators. EMBO J. **24**, 1874–1885.

Wu, Z.J., Irizarry, R.A., Gentleman, R., Martinez-Murillo, F., and Spencer, F. (2004). A model-based background adjustment for oligonucleotide expression arrays. J. Am. Stat. Assoc. **99**, 909–917.

Xi, W., Liu, C., Hou, X., and Yu, H. (2010). MOTHER OF FT AND TFL1 regulates seed germination through a negative feedback loop modulating ABA signaling in *Arabidopsis*. Plant Cell. **22**, 1733–1748.

Yilmaz, A., Mejia-Guerra, M.K., Kurz, K., Liang, X., Welch, L., and Grotewold, E. (2011). AGRIS: the Arabidopsis Gene Regulatory Information Server, an update. Nucleic Acids Res. **39**, D1118–D1122.

Zhu, S., Jeong, R.D., Venugopal, S.C., Lapchyk, L., Navarre, D., Kachroo, A., and Kachroo, P. (2011). SAG101 forms a ternary complex with EDS1 and PAD4 and is required for resistance signaling against turnip crinkle virus. PLoS Pathogens. **7**, e1002318.